SECURITY INFORMATION

CONFIDENTIAL

Copy 284
RM L53H18

NACA RM L53H18

NACA

RESEARCH MEMORANDUM

A TRANSONIC WIND-TUNNEL INVESTIGATION OF THE LONGITUDINAL STABILITY AND CONTROL CHARACTERISTICS OF A 0.09-SCALE MODEL OF THE BELL X-5 RESEARCH AIRPLANE AND COMPARISON WITH FLIGHT

By Ralph P. Bielat and George S. Campbell

Langley Aeronautical Laboratory
Langley Field, Va.

CLASSIFICATION CHANGED TO UNCLASSIFIED

AUTHORITY: RESEARCH ABSTRACT NO. 102

DATE: JUNE 22, 1956 WHL

CLASSIFIED DOCUMENT

This material contains information affecting the National Defense of the United States within the meaning of the espionage laws, Title 18, U.S.C., Secs. 793 and 794, the transmission or revelation of which in any manner to an unauthorized person is prohibited by law.

NATIONAL ADVISORY COMMITTEE
FOR AERONAUTICS

WASHINGTON
October 28, 1953

CONFIDENTIAL

NATIONAL ADVISORY COMMITTEE FOR AERONAUTICS

RESEARCH MEMORANDUM

A TRANSONIC WIND-TUNNEL INVESTIGATION OF THE LONGITUDINAL STABILITY AND CONTROL CHARACTERISTICS OF A 0.09-SCALE MODEL OF THE BELL X-5 RESEARCH AIRPLANE AND COMPARISON WITH FLIGHT

By Ralph P. Bielat and George S. Campbell

SUMMARY

An investigation was conducted in the Langley 8-foot transonic tunnel to determine the longitudinal stability and control characteristics of a 0.09-scale model of the Bell X-5 research airplane. The tests were made with the wing swept back 60° only. Lift, drag, pitching-moment, elevator hinge-moment, and pressure-distribution results are presented for Mach numbers varying from 0.60 to 1.10 and Reynolds numbers, based on the wing mean aerodynamic chord, varying from 2.86×10^6 to 3.56×10^6. The wind-tunnel results and dynamic-response calculations based on wind-tunnel data are compared with flight data.

The most significant results obtained in the present investigation concern the reduction in static longitudinal stability for the complete model configuration at lift coefficients in the vicinity of 0.5 for all test Mach numbers. Although the pitching-moment nonlinearities appeared to be rather moderate in comparison with instabilities shown for other swept-wing configurations, they were shown by dynamic-response calculations to be sufficiently severe to cause an undesirable pitch-up.

The large increase in zero-lift drag at transonic Mach numbers may be attributed to the rapid rates of development of cross-sectional area for the configuration and to the large maximum area associated with the relatively low equivalent fineness ratio.

A comparison of the wind-tunnel results with flight data indicated good agreement of lift, drag, and elevator deflection required for trim. Dynamic-response calculations based on wind-tunnel data predicted a pitch-up motion of the airplane that was in good agreement with flight results.

INTRODUCTION

The Bell X-5 is a research airplane whose angle of wing sweep may be varied in flight from approximately 20° to 60°. The airplane is used to obtain aerodynamic data in flight at transonic speeds on the effects of variable sweep.

The flight acceptance tests of the Bell X-5 research airplane indicated a pitch-up instability at lift coefficients of about 0.60 for all wing sweep angles and flight speeds. It was decided that the first of the detailed flight tests undertaken by the NACA would be made with the wings swept back 60°. In order to isolate the static characteristics of the airplane from the dynamic characteristics and to obtain more detailed aerodynamic information than could be obtained in flight, a 0.09-scale model of the Bell X-5 with the wings swept back 60° was tested in the Langley 8-foot transonic tunnel.

The results reported herein consist of lift, drag, pitching-moment, and elevator hinge-moment measurements for a Mach number range of 0.60 to 1.10. Total-pressure and static-pressure measurements were taken at the exit of the jet-engine duct to determine mass flow, inlet-velocity ratio, and internal drag coefficient. Static-pressure measurements over the nose inlet and the canopy were also taken. The static wind-tunnel data have been used to calculate the dynamic-response behavior of the airplane. Wherever possible, the wind-tunnel data have been compared with flight results presented in references 1 to 3.

SYMBOLS

The results of the investigation are presented in terms of standard NACA coefficients and are referred to the wind axes.

A	area
b	wing span
$\bar{c}$	mean aerodynamic chord of wing
C_D	drag coefficient, $D/q_\infty S$
C_{D_I}	internal drag coefficient of duct based on wing area

C_h elevator hinge-moment coefficient, $H/2q_\infty M_e$

C_{h_α} rate of change of elevator hinge-moment coefficient with angle of attack, $\partial C_h/\partial\alpha$

C_{h_δ} rate of change of elevator hinge-moment coefficient with elevator deflection, $\partial C_h/\partial\delta$

C_L lift coefficient, $L/q_\infty S$

C_{L_α} lift-curve slope, $dC_L/d\alpha$

C_{N_A} airplane normal-force coefficient

C_m pitching-moment coefficient, $M_{cg}/q_\infty S\bar{c}$

C_{m_q} damping derivative resulting from steady pitching velocity, $\partial C_m \Big/ \partial \frac{q\bar{c}}{2V}$

$C_{m_{\dot{\alpha}}}$ damping derivative resulting from rate of change of angle of attack, $\partial C_m \Big/ \partial \frac{\dot{\alpha}\bar{c}}{2V}$

$C_{m_{i_t}}$ stabilizer effectiveness parameter, $\partial C_m/\partial i_t$

C_{m_δ} elevator effectiveness parameter, $\partial C_m/\partial\delta$

D drag

g acceleration due to gravity

H elevator hinge moment

h_p pressure altitude

i_t stabilizer incidence referred to center line of thrust, positive when trailing edge is down

I_y moment of inertia about airplane pitch axis through center of gravity; 8860 slug-ft^2

L lift

L/D	lift-drag ratio
l_t	tail length
m	airplane mass
m'	mass-flow rate, ρAV
M	Mach number
M_{cg}	pitching moment of aerodynamic forces about lateral axis which passes through center-of-gravity location at $0.464\bar{c}$ at point 1.706 inches above center line of thrust, model scale
M_e	area moment of elevator about its hinge line
n	normal load factor
P	pressure coefficient, $\frac{p - p_\infty}{q_\infty}$
p	local static pressure
p_∞	free-stream static pressure
q	airplane pitching velocity
q_∞	free-stream dynamic pressure, $\frac{1}{2}\rho_\infty V_\infty^2$
R	Reynolds number based on $\bar{c}$
S	wing area
t	time
u	dimensionless velocity, V/V_1
V	velocity
W	airplane weight, 9,000 lb
W'	dimensionless weight parameter (level flight lift coefficient), $2W/\rho V_1^2 S$

α angle of attack referred to center line of thrust

$\dot{\alpha},\ddot{\alpha}$ differentiation of angle of attack with respect to time

ϵ effective downwash angle

δ elevator deflection measured in plane perpendicular to hinge line, positive when trailing edge is down

ν dynamic response parameter, $\rho V_1^2 S\bar{c}/2I_y$

ρ air density

τ airplane time factor, $m/\rho S V_1$

Subscripts:

1 designates an initial value

o designates the curve defining static variation of the coefficients C_m, C_L, and C_D with α when the controls are fixed in their initial positions i_{t_1} and δ_1

∞ free stream

i nose-inlet entrance

APPARATUS AND MODEL

Tunnel

The investigation was conducted in the Langley 8-foot transonic tunnel which has a dodecagonal cross section and is a slotted-throat, single-return type of wind tunnel. The use of longitudinal slots along the test section permitted the testing of the model at speeds continuously variable through the speed of sound without the usual choking effects found in the conventional closed-throat type of wind tunnel. A more complete description of the Langley 8-foot transonic tunnel can be found in reference 4.

Model

The model employed for the present investigation was a 0.09-scale model of the Bell X-5 research airplane. The model was constructed of

steel and was supplied to the NACA by the Bell Aircraft Corporation. The X-5 airplane is a research airplane whose wing angle of sweep is variable in flight from 20° to 60°. There was also longitudinal translation of the wing with respect to the fuselage as the angle of sweep varied.

Three-view drawings and physical characteristics of the model are presented in figure 1. It was necessary to modify the model at the rear end of the fuselage since the model was supported in the tunnel by means of a sting-support system. The horizontal and vertical tail surfaces on the model, therefore, correspond to a slightly different configuration than exists for the full-scale airplane. A comparison of the modified fuselage and empennage with the full-scale airplane is made in figure 1. A photograph of the model on the sting support is shown in figure 2.

Control deflections were accomplished by providing several control surfaces with fixed angles of deflection. The control surfaces were of the plain-flap, unsealed type. All control surfaces were restrained by beams incorporating electrical strain gages.

The jet-engine ducting was simulated on the model by the use of a straight-through, constant-area duct extending from the nose to the jet exit.

The model was attached to the sting support through a six-component internal electrical strain-gage balance. The angle of attack of the model was varied by pivoting the sting support about an axis approximately 66 inches downstream of the center-of-gravity location on the model. In order to keep the model position reasonably close to the tunnel axis when the model angle of attack was varied from 12° to 28°, a 20° coupling was inserted upstream of the pivot point. The angle-of-attack mechanism was remotely controlled which permitted angle-of-attack changes while the tunnel was operating.

A pendulum-type inclinometer, calibrated against angle of attack of the model, and located within the fuselage of the model permitted the angle of attack to be set within ±0.1° at all test Mach numbers.

TESTS

The Reynolds number based on the mean aerodynamic chord of the wing and averaged for several runs is shown in figure 3 as a function of test

Mach number. The Reynolds number varied from 2.86×10^6 to 3.56×10^6 for the present investigation.

Measurements

Lift, drag, and pitching moment were determined by means of an electrical strain-gage balance located inside the fuselage. The measurements were taken for angles of attack from -2° to 28° at Mach numbers varying from 0.60 to 0.93 and from -2° to the highest angle permissible as determined by the design pitching-moment limit of the balance for Mach numbers of 0.96 to 1.10. Elevator hinge moments were determined by means of electrical strain gages. The measurements were obtained for elevator deflections varying from 2° to -14° for the same range of angles of attack and Mach numbers as for the lift, drag, and pitching-moment measurements. Total-pressure and static-pressure measurements were taken at the exit of the jet-engine duct to determine the mass flow, inlet-velocity ratio, and internal drag coefficient. In addition, static-pressure measurements were made over the nose inlet and canopy. These measurements were taken for angles of attack from -2° to 8° at Mach numbers varying from 0.60 to 1.12.

No attempt was made to control the flow quantity through the jet-engine duct during the present investigation.

The data presented herein were obtained on the model with the wing swept back 60°.

Corrections and Accuracy

No corrections to the free-stream Mach number and dynamic pressure for the effects of model and wake blockage and to the drag coefficient for the effect of the pressure gradient caused by the wake are necessary for tests in the slotted test section of the Langley 8-foot transonic tunnel (ref. 5). There is a range of Mach numbers above a Mach number of 1.00, however, where the data are affected by reflected compressions and expansions from the test-section boundary. Based on the results of reference 6, it is believed that for Mach numbers up to approximately 1.03 the effects of these disturbances on the measurements made in the present investigation may be considered to be negligible. For test Mach numbers above 1.03, however, the data were influenced by the boundary-reflected disturbances, but the extent to which the data were affected by the reflected disturbances is not known for these tests. In the plots of drag coefficient against Mach number, however, there is shown by dashed lines above a Mach number of 1.03 an estimated variation of drag coefficient which is believed to be typical of the correct variation based on the studies of reference 7.

The drag data have been corrected for base pressure such that the drag corresponds to conditions where the base pressure is equal to the free-stream static pressure.

Static calibration tests were made of the elevator to permit correction for elevator deflection under load; these corrections, although found to be small, have been applied to the hinge-moment data.

No corrections for the forces and moments produced by the sting interference have been applied to the data. As indicated in reference 8 the significant corrections would be limited to small increments in pitching moment and drag and to the effective downwash angle.

The estimated consistency of the data at a Mach number of 0.60, based on the static calibrations and the reproducibility of the data, is as follows:

C_L	± 0.01
C_D	± 0.001
C_m	± 0.006
C_h	± 0.005

These errors would be inversely proportional to the dynamic pressure and therefore would be lower at the higher Mach numbers.

RESULTS AND DISCUSSION

This portion of the paper has been arranged into several sections for presenting the results of the present investigation: lift and drag characteristics; static longitudinal stability and control characteristics; airplane time histories calculated from the static wind-tunnel data; elevator hinge-moment characteristics; mass-flow characteristics and limited pressure distributions. Whenever possible, the wind-tunnel results have been compared with available flight data.

Lift and Drag Characteristics

The effects of stabilizer incidence and of elevator deflection on the aerodynamic characteristics of the model are given in figures 4, 5, and 6. Nonlinearities in the lift characteristics below the stall were indicated throughout the Mach number range but became less marked for Mach numbers above 0.96. For Mach numbers of 0.60 to 0.85, the variation of lift coefficient with angle of attack showed well-defined stall characteristics, but as the Mach number was increased to higher values, the stall became less pronounced. The data also indicated that maximum

lift had not been reached at the higher Mach numbers even though the data were obtained for angles of attack near 20° to 28°.

The variation of lift-curve slope with Mach number for the complete model is given in figure 7. The values of the lift-curve slope were averaged over the lift-coefficient range from 0 to 0.30. The lift-curve slope had a value of 0.045 at a Mach number of 0.60 and increased to a maximum value of 0.057 at a Mach number of 1.06.

Comparisons of flight data and wind-tunnel data on the variation of normal-force coefficient with angle of attack for several Mach numbers are made in figure 8. Two types of flight maneuvers were performed to obtain the data; one maneuver consisted of elevator deflections in accelerated turns and the second maneuver consisted of stabilizer pull-ups. The wind-tunnel data were selected for elevator deflections and stabilizer deflections corresponding to the control-positions recorded in flight. In general, it can be seen that the agreement between the wind-tunnel data and the flight data is good for Mach numbers up to approximately 0.85. At Mach numbers 0.90 to 0.96 the agreement for the low angle-of-attack range (4° to 12°) is good; however, the normal-force coefficient measured in the wind tunnel at high angles of attack continues to increase with increase in angle of attack, whereas it has appeared that maximum normal-force coefficient has been reached in flight. Although the reasons for this disparity in the data are not obvious, it is believed that the differences could be due in part to the effects of Reynolds number on maximum lift.

The effect of compressibility on the drag at zero lift is shown in figure 9. The drag rise $\left(\text{defined as the value where } \frac{dC_D}{dM} = 0.1\right)$ occurred at a Mach number of 0.91. The rate of drag increase with Mach number and the drag-rise increment were large and unlike that which would be expected for a 60° sweptback wing (see, for example, ref. 9). The large drag-rise increment is believed to be due to the shape of the fuselage. As discussed in reference 10, the drag-rise increment near the speed of sound of wing-body combinations can be related to the axial development of the cross-sectional area normal to the airstream. It was also shown that variations of configurations which resulted in less rapid rates of development of cross-sectional area, as well as reductions of the relative magnitude of the maximum areas (increases in effective fineness ratio), decreased the drag-rise increments near the speed of sound. The axial distribution of the cross-sectional area for the fuselage and canopy and for the wing is presented in figure 10. The cross-sectional area of the configuration was reduced by subtracting the equivalent free-stream tube area of the internal flow measured at a Mach number of 1.00. The contribution of the cross-sectional area of the wing is small when compared with that of the fuselage; however, it can be seen from figures 1 and 10 that the fuselage shape corresponds

to an area diagram which has large slopes fore and aft. The equivalent fineness ratio of the area diagram is 5.8 with the maximum area occurring at approximately 40 percent of the fuselage length. The low equivalent fineness ratio of the configuration (compared with an optimum body of revolution of fineness ratio 9.0) could thus account for the large drag-rise increment shown in figure 9.

Comparisons of the drag coefficients measured in flight with the wind-tunnel drag measurements are made in figure 11. The wind-tunnel drag data were selected for elevator and stabilizer deflections corresponding to the control-positions used in flight. In general, in the range of Mach numbers 0.75 to 0.93 the agreement was good between the drag coefficients measured in flight and in the wind tunnel for most of the lift-coefficient range shown. At Mach numbers 0.60 and 0.96, and lift coefficients to 0.40, however, considerable discrepancy exists between the measured flight drag and wind-tunnel drag which could be due partially to the difficulties encountered in measuring drag in flight (ref. 1).

The drag measurements near a lift coefficient of 0.20 at Mach numbers 1.00 and 1.03 shown in figure 11 were obtained in flight by diving the airplane in shallow dives. The flight results at a lift coefficient of 0.2 are compared with the wind-tunnel data through the Mach number range in figure 12. Again it can be seen that the agreement of the data is quite good. The measured flight drag and wind-tunnel drag indicated approximately the same drag-rise Mach number and same drag-rise increment near the speed of sound. The estimated variation of drag coefficient with Mach number for the wind-tunnel data as shown by the small dashed curve and discussed previously shows an even better agreement of the drags for the flight and wind-tunnel data.

The data of figures 4 and 6 were used to calculate the trimmed lift-to-drag ratios of the model at various Mach numbers and these results are presented in figure 13 as a function of lift coefficient. It can be seen that the lift coefficient for maximum L/D increased from a value of 0.20 at a Mach number of 0.60 to approximately 0.45 at a Mach number of 1.10. It can also be noted that the available maximum L/D dropped abruptly above a Mach number of 0.93. The variation with Mach number of the trimmed $(L/D)_{max}$ is shown in figure 14. The values of trimmed lift-drag ratio for level flight at sea level and an altitude of 35,000 feet for a wing loading of 48.5 pounds per square foot are also shown in figure 14. The advantages to be gained by proper selection of flight altitude are clearly indicated.

Longitudinal Stability and Control Characteristics

Static longitudinal stability.- The effects of stabilizer incidence and of elevator deflection on the pitching-moment characteristics of th

model are presented in figures 4 and 6, respectively. For the stabilizer-incidence tests, the pitching-moment coefficients have been plotted against angle of attack (fig. 5) as well as against lift coefficient in order to facilitate the interpretation of the nonlinear characteristics of the curves. The wing-fuselage configuration (fig. 4) showed marked pitch-up characteristics at lift coefficients above 0.4 for Mach numbers up to 0.96 and no pitch-up was indicated at Mach numbers 1.00 to 1.10. The addition of the tail to the model reduced the magnitude of the pitch-up at the lower Mach numbers such that the model was about neutrally stable at lift coefficients of the order of 0.6 to 0.8 for Mach numbers up to 0.85. With an increase in Mach number to approximately 1.03, however, the model exhibited an abrupt pitch-up instability over a smaller lift-coefficient range. In the range of high angles of attack (see fig. 5), the model regained its stability at all speeds because of a decrease of downwash at the tail.

The variation with Mach number of the elevator deflection required for trim for idle-power conditions for the model is shown in figure 15(a). The elevator deflections required for trim were estimated from the wind-tunnel data for assumed conditions of level flight at an altitude of 42,000 feet. Control-position instability is indicated for Mach numbers 0.96 to 1.02. The control-position instability is due primarily to the changes in the out-of-trim pitching-moment coefficients as shown in figure 16 and to a lesser extent to the changes in the control-effectiveness parameter C_{m_δ} presented in figure 17. The changes in trim, however, do not appear to be particularly severe through the transonic speed range.

A comparison of the wind-tunnel data with flight data on the elevator deflection required for trim is also made in figure 15(a). The variation with Mach number of the elevator deflection required for trim measured in flight, however, was obtained at 100-percent power conditions. A few flight tests have been made to determine the effects of power on the elevator deflection required for trim and these effects are shown in figure 15(b). Both the wind-tunnel data and the flight data showed control-position instability to occur at approximately a Mach number of 0.96.

Control effectiveness.- The effects of compressibility on the control-effectiveness parameters C_{m_δ} and $C_{m_{i_t}}$ are shown in figure 17. The values of the parameters were averaged over a lift-coefficient range from 0 to 0.3. The stabilizer-effectiveness parameter $C_{m_{i_t}}$ increased through the transonic speed range whereas the elevator-control-effectiveness parameter C_{m_δ} indicated a 33-percent decrease in the transonic speed range. Although there was a decrease in the elevator control effectiveness, the control still appears to be adequate since, as indicated in figure 6, the elevator can produce changes in trim to a lift coefficient of 0.33.

Control maneuvering effectiveness.- The control maneuvering effectiveness of the elevator is shown in figure 18 as the amount of elevator deflection required to trim for various accelerated-flight conditions at sea level and an altitude of 35,000 feet. The additional elevator deflection required to offset the damping in pitch as calculated by the method given in reference 11 is included in the results given in figure 18. The control maneuvering effectiveness showed a gradual increase as the speed was increased up to a Mach number of 0.93 followed by a rapid decrease through the transonic speed range. There was no indication of control maneuvering instability at sea level inasmuch as the lift coefficients corresponding to the accelerated-flight conditions examined were below the pitch-up instability. At an altitude of 35,000 feet, however, control maneuvering instability was indicated. As an example, control maneuvering instability occurred between the 2g to 4g accelerated-flight conditions for Mach numbers between 0.94 and 1.01. For sea-level flight conditions, only about 2° of elevator deflection is required to produce a 4g acceleration at a Mach number of 0.95. Approximately 11° of elevator deflection is required to produce a similar acceleration at a Mach number of 0.95 at an altitude of 35,000 feet.

Effective downwash characteristics.- The variation of effective downwash angle with angle of attack is shown in figure 19. The effective downwash angle at a given angle of attack was determined by finding the model stabilizer incidence at which the pitching-moment coefficient of the complete model configuration was equal to that of the complete model configuration less the horizontal tail (see fig. 5). The sum of the model angle of attack and the stabilizer incidence thus found gave the effective downwash angle in the region of the horizontal tail. The effect of the horizontal-tail drag on the pitching moment was neglected. Since only three stabilizer-incidence settings were used, some of the data at the low and at the high angles of attack given in figure 19 were extrapolated. The decrease in the effective downwash angle at high angles of attack was responsible for the large increase in the longitudinal stability of the model as was previously discussed.

Figure 20 presents the effect of Mach number on the rate of change of effective downwash angle with angle of attack averaged for angles of attack from -2° to 6°. No large changes in the downwash derivative $\partial\epsilon/\partial\alpha$ were indicated through the transonic speed range.

Dynamic-Response Calculations

The static pitching-moment nonlinearities in the present paper are relatively mild when compared with some of the instabilities presented in references 12 and 13 for various complete-model configurations. From such a casual inspection of the static pitching moments, it might be

expected that pitch-up would not be particularly severe for the X-5 airplane. However, the airplane was found to have marked pitch-up during recent flight tests (ref. 3). Dynamic response calculations were therefore made in order to determine the true significance of the pitching-moment nonlinearities.

The equations used for calculating airplane time histories have been derived from Newton's laws of motion in reference 14. The basic approach in the derivation was first to neglect changes in Mach number during a maneuver so that angle of attack and pitching velocity could be calculated from simple two-degree-of-freedom considerations. Then, the Mach number variation with time was calculated by taking into account the third degree of freedom describing the longitudinal motion of the airplane. The equations used for the calculations were

$$\ddot{\alpha} + \frac{1}{2\tau}\left(C_{L_\alpha} - \frac{C_{m_q} + C_{m_{\dot{\alpha}}}}{2K_y{}^2}\right)\dot{\alpha} - \nu C_{m_o} = \nu\left[C_{m_{i_t}}(i_t - i_{t_1}) + C_{m_\delta}(\delta - \delta_1)\right] \quad (1)$$

$$q = \frac{1}{2\tau}\left(C_{L_o} - W'\right) + \dot{\alpha} \quad (2)$$

$$u = \frac{1}{1 + \frac{1}{2\tau}\int_0^t C_{D_o}\, dt} \quad (3)$$

$$n = \frac{(C_L \cos\alpha + C_D \sin\alpha)u^2}{W'} \quad (4)$$

where radian measure has been used throughout. The damping derivatives C_{m_q} and $C_{m_{\dot{\alpha}}}$ were estimated from the static wind-tunnel data using the relations

$$C_{m_q} = 1.2\left(2\,\frac{l_t}{\bar{c}}\,C_{m_{i_t}}\right) \quad (5a)$$

$$C_{m_{\dot{\alpha}}} = 2 \frac{l_t}{\bar{c}} C_{m_{i_t}} \frac{\partial \epsilon}{\partial \alpha} \tag{5b}$$

Because the aerodynamic parameters in equation (1) had nonlinear variations with angle of attack for the X-5 airplane, numerical results were obtained by using the Runge-Kutta procedure described in reference 15.

Results of the dynamic-response calculations are presented in figures 21 and 22 and compared with flight results taken from reference 3. The character of the pitch-up is shown most clearly by the stabilizer maneuvers of figure 21, in which a linear variation of control position results in a decidedly nonlinear angle-of-attack response. In analyzing the character of the pitch-up, attention can be focused largely on angle of attack because the changes in normal load factor during a pitch-up are frequently softened as a result of a decrease in lift-curve slope at the higher angles of attack and a loss in speed during the maneuver (see fig. 21(c), for example). No matter how gradual the variation of normal load, however, an uncontrolled pitch-up to high angles of attack is always objectionable, particularly when accompanied by lateral and directional difficulties, as described in reference 3.

Based on the time histories, the point at which pitch-up commences is seen to be near 12° for Mach numbers between 0.76 and 0.91. A similar conclusion results from an inspection of the static pitching-moment data. While a cursory inspection of the static pitching moments indicated that the nonlinearities were relatively moderate in comparison with those for several other configurations, the dynamic calculations show that these nonlinearities were sufficient to cause a severe pitch-up. More explicitly, the maximum rate of change of angle of attack was about four times greater after the start of pitch-up than in the controlled part of the motion for a constant rate of stabilizer input.

In comparing the calculated time histories with flight results, it is seen that the peak angles of attack during the maneuvers were in all cases predicted within 2° or less. The poorer agreement between calculated and flight results shown for the elevator turns may be caused by the neglecting of cross coupling of lateral and longitudinal motions in the simplified equations of motion. However, a time displacement such as that shown in figure 22(b) is not considered important because the maximum values of α, n, and q were predicted satisfactorily.

Elevator Hinge-Moment Characteristics

The variation of hinge-moment coefficient with elevator deflection is presented in figure 23. Figures 24 and 25 show hinge-moment-coefficient

variation with angle of attack and hinge-moment-coefficient variation with Mach number for 0° angle of attack, respectively.

No large changes in the elevator hinge-moment coefficients occurred for small elevator deflections up to a Mach number of 1.03. (See fig. 25.) Marked changes in the hinge-moment characteristics occurred for all elevator deflections for Mach numbers greater than 1.03; the reasons for these changes are not clearly understood. Schlieren photographs (not presented herein) taken during the tests indicated no disturbances in the flow in the region of the elevator; however, a detached bow wave located ahead of the tail was visible at Mach numbers 1.06 and 1.10.

The variation of the hinge-moment parameters $(C_{h_\alpha})_{\delta=0^\circ}$ and $(C_{h_\delta})_{\alpha=0^\circ}$ with Mach number is shown in figure 26. These slopes are the average values for angles of attack from -2° to 2° and elevator deflections from 0° to -5°. In general, the hinge-moment parameters indicated little variation below a Mach number of 0.88. In the range of Mach numbers from 0.93 to 1.07 the hinge-moment parameter C_{h_α} showed a gradual change from negative to positive values. A large increase in the negative value of the hinge-moment parameter C_{h_δ} was noted at Mach numbers above 0.88.

Mass-Flow Characteristics and Pressure Distributions

The results of the mass-flow measurements for the jet-engine duct are presented in figures 27 to 29. The variation of mass-flow ratio with Mach number for 0° angle of attack for the jet-engine duct is shown in figure 27. The mass-flow ratio increased from a value of 0.86 at a Mach number of 0.60 to 0.88 at a Mach number of 1.12. In comparison, mass-flow ratios of the order of 0.90 to 0.85 were measured in flight for Mach numbers 0.80 to 0.96.

The variation of inlet-velocity ratio with Mach number for 0° angle of attack is given in figure 28. The inlet-velocity ratio decreased from a value of 0.80 to 0.62 as the Mach number increased from 0.60 to 1.12.

The variation of the internal drag coefficient based on wing area with angle of attack presented in figure 29 indicates that C_{D_I} was invariant with angle of attack. It will be noted that the internal drag of the jet-engine duct was small and therefore would have a small effect on the total drag values presented herein. It will also be noted that the effects of compressibility on the internal drag coefficient are negligible.

The surface pressure distributions measured over the nose and canopy of the model for angles of attack of 0°, 4°, and 8°, and for Mach numbers of 0.60, 0.90, 1.00, and 1.10 are presented in figure 30. There was no pronounced peak pressure development over the lip of the upper surface of the nose inlet for the angle of attack and Mach number range shown. This was probably due in part to the large nose radius of the upper surface of the nose inlet and in part to the high inlet-velocity ratio. It should also be noted that the measured pressures on the external and internal surfaces over the upper surface of the nose inlet remained positive for the range of angles and Mach numbers presented. On the other hand, the development of large peak negative pressures on the external surface of the side and lower surface of the nose inlet were indicated. In some instances, the maximum peak negative pressures developed are not shown because the magnitude of the pressures were such as to cause the fluid in the manometer board to exceed the height of the column.

The pressures measured over the canopy (fig. 30) indicated a rather abrupt pressure gradient in a region 5.5 to 6.0 inches from the model nose. For Mach numbers 0.90 to 1.10, supercritical velocities existed over an extensive region on the canopy for the angle-of-attack range presented.

CONCLUSIONS

An investigation was made in the Langley 8-foot transonic tunnel of the longitudinal stability and control characteristics of a 0.09-scale model of the Bell X-5 research airplane. Tests were made for the model with the wing swept back 60° only. The following conclusions are indicated:

1. One of the most significant results obtained in the present investigation concerns the reduction in static longitudinal stability for the complete model configuration at lift coefficients in the vicinity of 0.5 for all test Mach numbers. Although the pitching-moment nonlinearities appear to be rather moderate in comparison with instabilities shown for other swept-wing configurations, they were shown by dynamic-response calculations to be sufficiently severe to cause an undesirable pitch-up.

2. The elevator deflections required for trimmed level flight indicated control-position instability at transonic Mach numbers although the trim changes were not too severe.

3. The control maneuvering effectiveness of the elevator showed a gradual increase as the speed increased up to a Mach number of 0.93 followed by a rapid decrease through the transonic speed range.

4. The value of trimmed maximum lift-drag ratio fell off abruptly at transonic Mach numbers, decreasing from 7.2 at $M = 0.90$ to 3.5 at $M = 1.05$.

5. The large increase in zero-lift drag at transonic Mach numbers may be attributed to the rapid rates of development of cross-sectional area for the configuration and to the large maximum area associated with the relatively low equivalent fineness ratio of the configuration.

6. In the range of Mach numbers from 0.93 to 1.07 the hinge-moment parameter C_{h_α} showed a gradual change from negative to positive values and a large increase in the negative value of the hinge-moment parameter C_{h_δ} was noted at Mach numbers above 0.88.

7. The wind-tunnel results have been compared with flight data wherever possible. The comparisons of lift, drag, and elevator deflection required for trim were in good agreement. Dynamic-response calculations based on wind-tunnel data predicted a pitch-up motion of the airplane that was in good agreement with flight results.

Langley Aeronautical Laboratory,
National Advisory Committee for Aeronautics,
Langley Field, Va., August 14, 1953.

REFERENCES

1. Bellman, Donald R.: Lift and Drag Characteristics of the Bell X-5 Research Airplane at 59° Sweepback for Mach Numbers From 0.60 to 1.03. NACA RM L53A09c, 1953.

2. Finch, Thomas W., and Briggs, Donald W.: Preliminary Results of Stability and Control Investigation of the Bell X-5 Research Airplane. NACA RM L52K18b, 1953.

3. Finch, Thomas W., and Walker, Joseph A.: Static Longitudinal Stability of the Bell X-5 Research Airplane With 59° Sweepback. NACA RM L53A09b, 1953.

4. Wright, Ray H., and Ritchie, Virgil S.: Characteristics of a Transonic Test Section With Various Slot Shapes in the Langley 8-Foot High-Speed Tunnel. NACA RM L51H10, 1951.

5. Wright, Ray H., and Ward, Vernon G.: NACA Transonic Wind-Tunnel Test Sections. NACA RM L8J06, 1948.

6. Ritchie, Virgil S., and Pearson, Albin O.: Calibration of the Slotted Test Section of the Langley 8-Foot Transonic Tunnel and Preliminary Experimental Investigation of Boundary-Reflected Disturbances. NACA RM L51K14, 1952.

7. Whitcomb, Charles F., and Osborne, Robert S.: An Experimental Investigation of Boundary Interference on Force and Moment Characteristics of Lifting Models in the Langley 16- and 8-Foot Transonic Tunnels. NACA RM L52L29, 1953.

8. Osborne, Robert S.: High-Speed Wind-Tunnel Investigation of the Longitudinal Stability and Control Characteristics of a 1/16-Scale Model of the D-558-2 Research Airplane at High Subsonic Mach Numbers and at a Mach Number of 1.2. NACA RM L9C04, 1949.

9. Wood, Raymond B., and Fleming, Frank F.: A Transonic-Wing Investigation in the Langley 8-Foot High-Speed Tunnel at High Subsonic Mach Numbers and at a Mach Number of 1.2. Wing-Fuselage Configuration Having a Wing of 60° Sweepback, Aspect Ratio 4, Taper Ratio 0.6, and NACA 65A006 Airfoil Section. NACA RM L50J25, 1951.

10. Whitcomb, Richard T.: A Study of the Zero-Lift Drag-Rise Characteristics of Wing-Body Combinations Near the Speed of Sound. NACA RM L52H08, 1952.

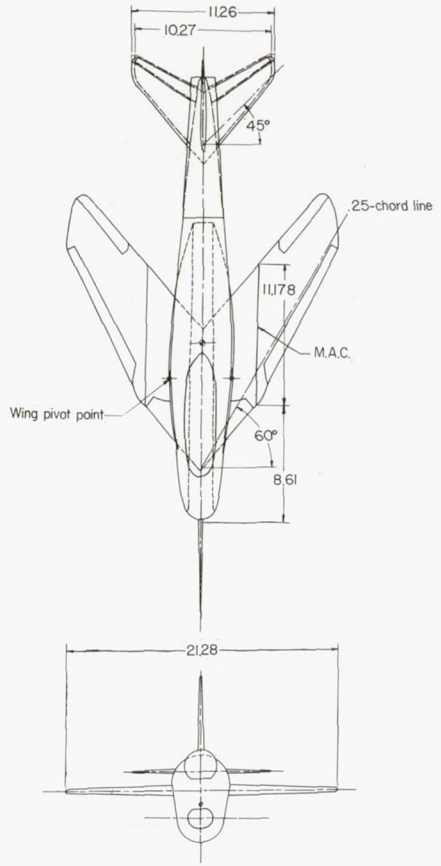
11. Phillips, William H.: Appreciation and Prediction of Flying Qualities. NACA Rep. 927, 1949. (Supersedes NACA TN 1670.)

12. Morrison, William D., Jr., and Alford, William J., Jr.: Effects of Horizontal-Tail Height and a Wing Leading-Edge Modification Consisting of a Full-Span Flap and Partial-Span Chord-Extension on the Aerodynamic Characteristics in Pitch at High Subsonic Speeds of a Model With a 45° Sweptback Wing. NACA RM L53E06, 1953.

13. Weil, Joseph, Sleeman, William C., Jr., and Byrnes, Andrew L., Jr.: Investigation of the Effects of Wing and Tail Modifications on the Low-Speed Stability Characteristics of a Model Having a Thin 40° Swept Wing of Aspect Ratio 3.5. NACA RM L53C09, 1953.

14. Campbell, George S., and Weil, Joseph: The Interpretation of Nonlinear Pitching Moments In Relation to the Pitch-Up Problem. NACA RM L53I02, 1953.

15. Scarborough, James B.: Numerical Mathematical Analysis. Second ed., The Johns Hopkins Press (Baltimore), 1950.



Physical characteristics of model

Wing:

Airfoil section perpendicular to 38.02-percent-chord line	
Pivot point	NACA 64(10)A011
Tip	NACA 64(08)A008.28
Area, sq ft	1.513
Aspect ratio	1.94
Taper ratio	0.423
Incidence, deg	0
Dihedral, deg	0
Geometric twist, deg	0

Horizontal tail:

Airfoil section parallel to plane of symmetry	NACA 65A006
Area, sq ft	0.284
Aspect ratio	2.94

Vertical tail:

Airfoil section parallel to aft fuselage center line	NACA 65A006
Area, sq ft	0.225
Aspect ratio	1.51

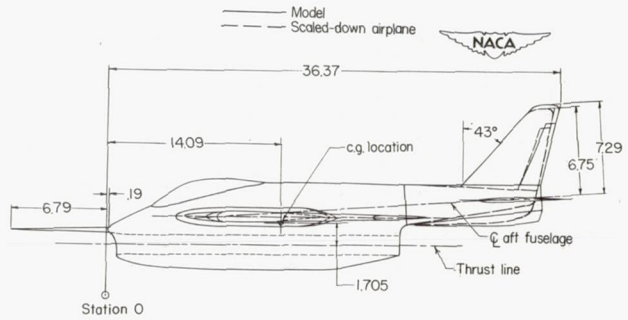
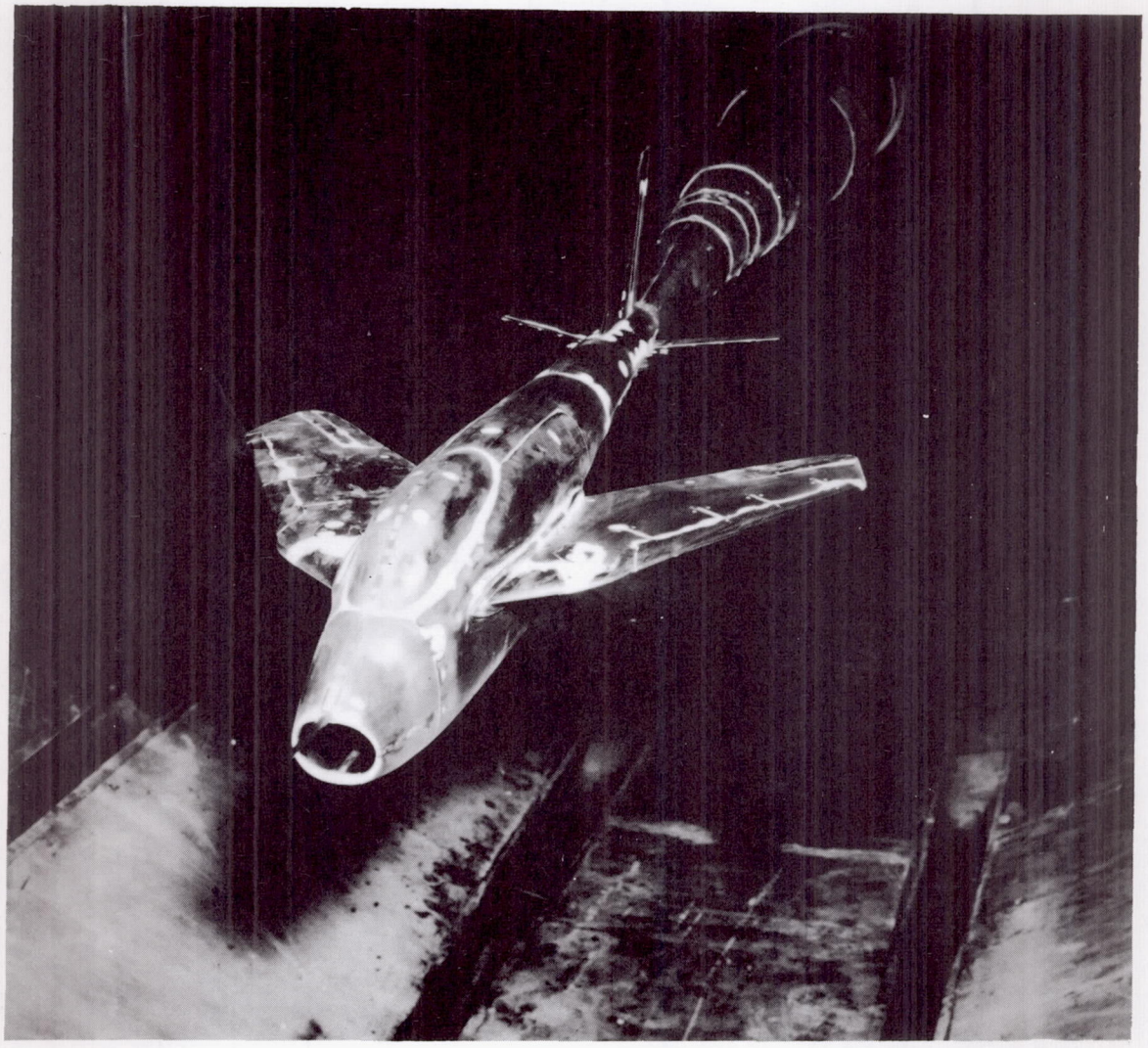


Figure 1.- General arrangement of test model. All dimensions in inches except as noted.



L-75523

Figure 2.- Test model on sting support.

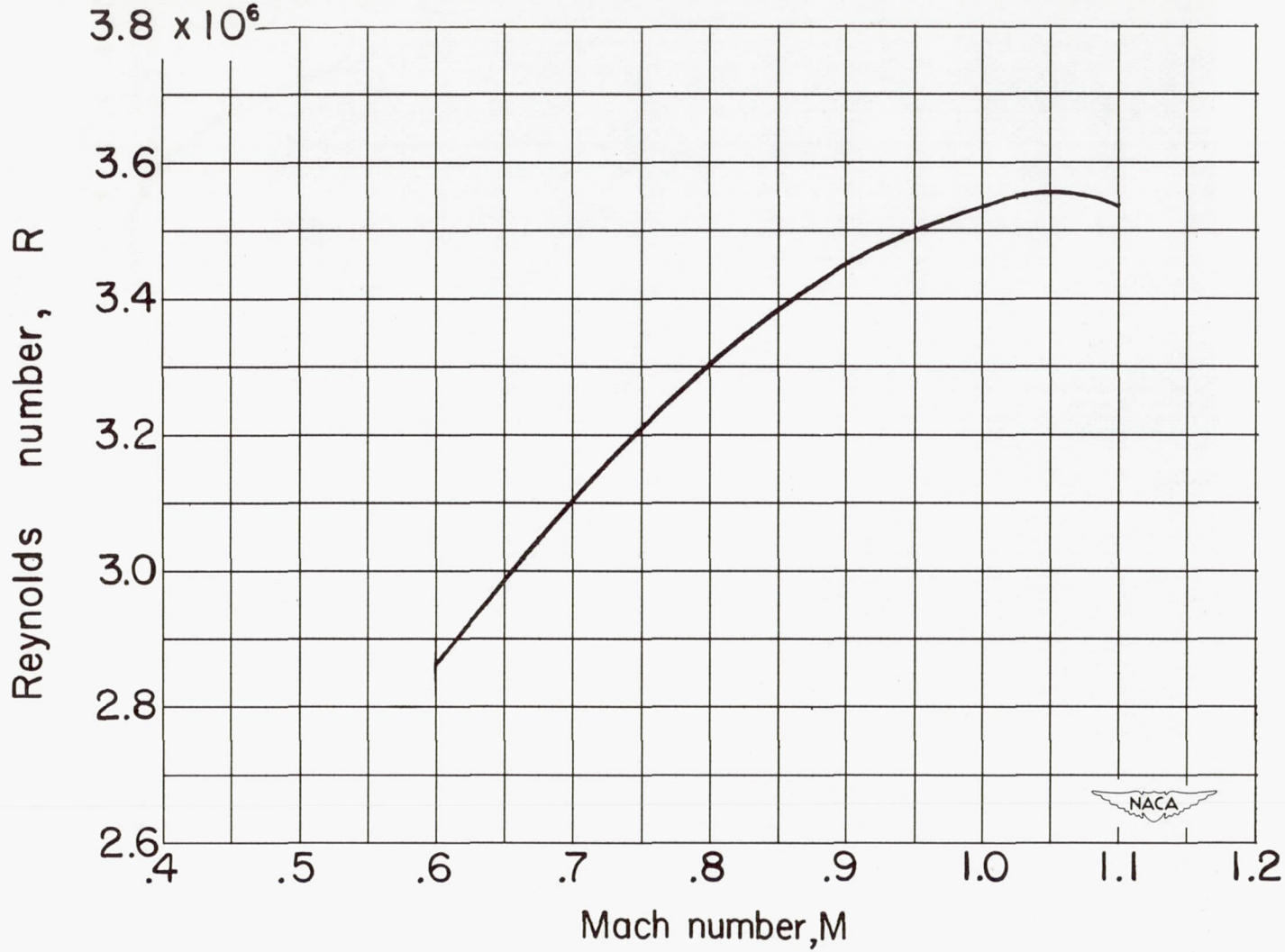
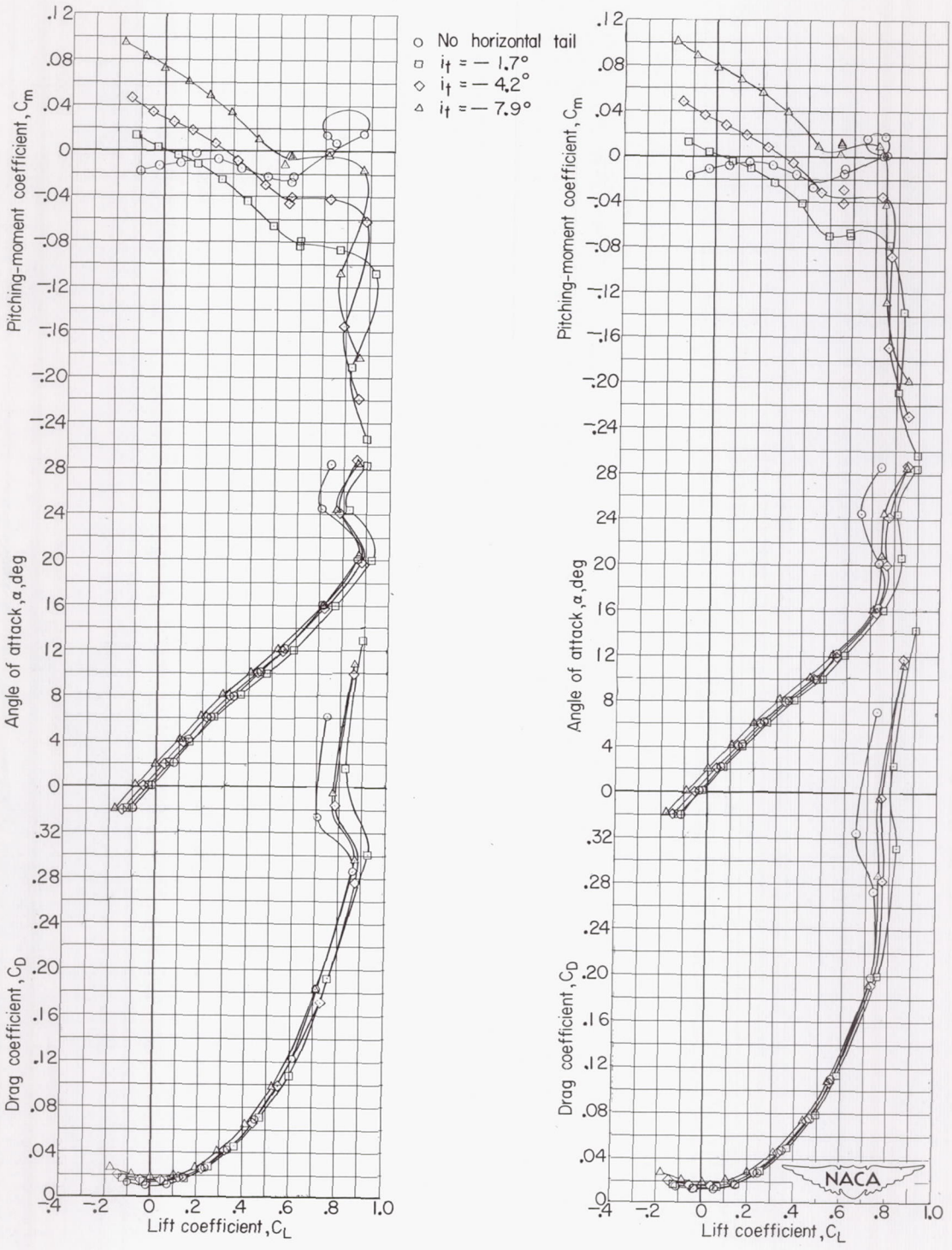
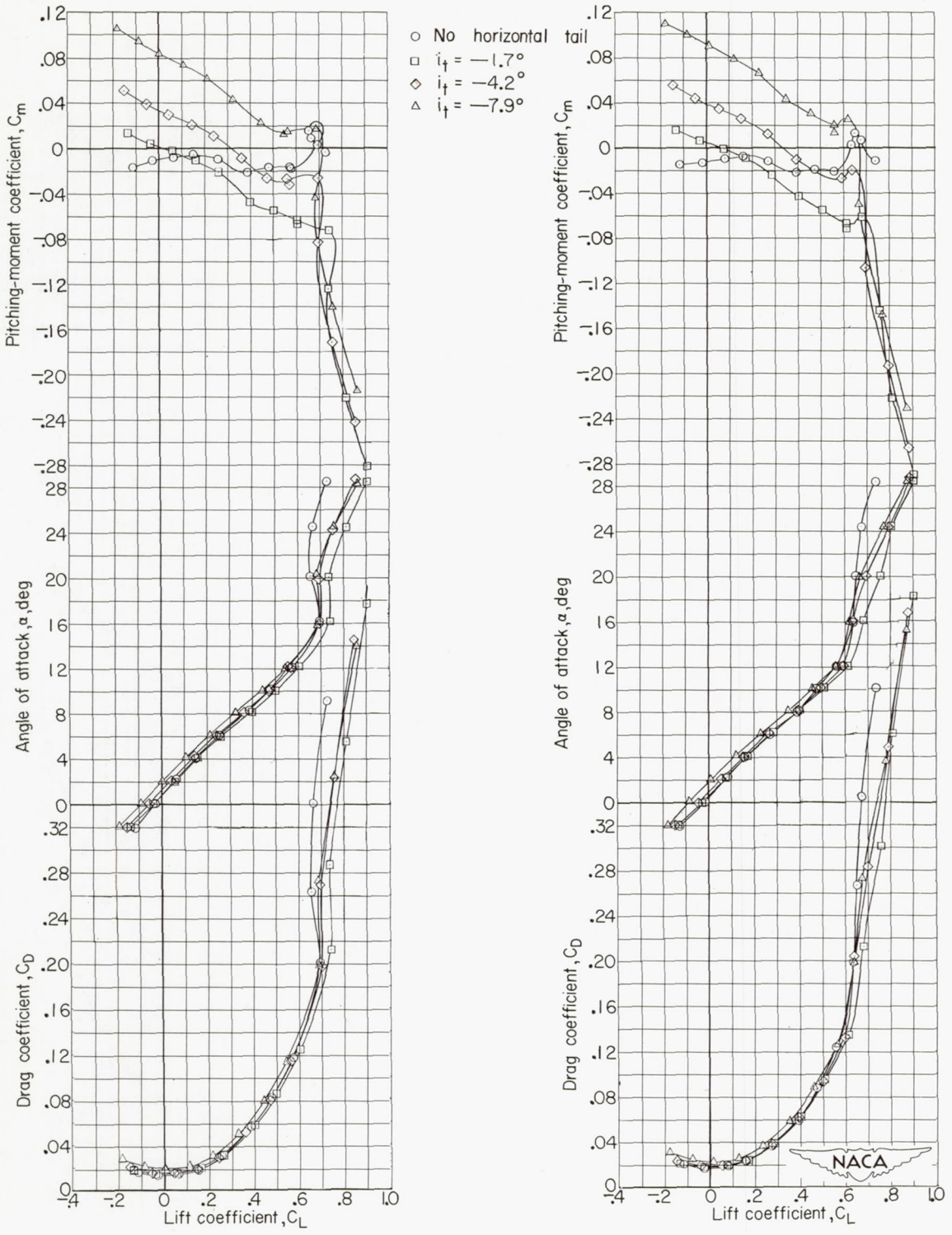


Figure 3.- Variation with Mach number of test Reynolds number based on wing mean aerodynamic chord.



(a) M = 0.60. (b) M = 0.75.

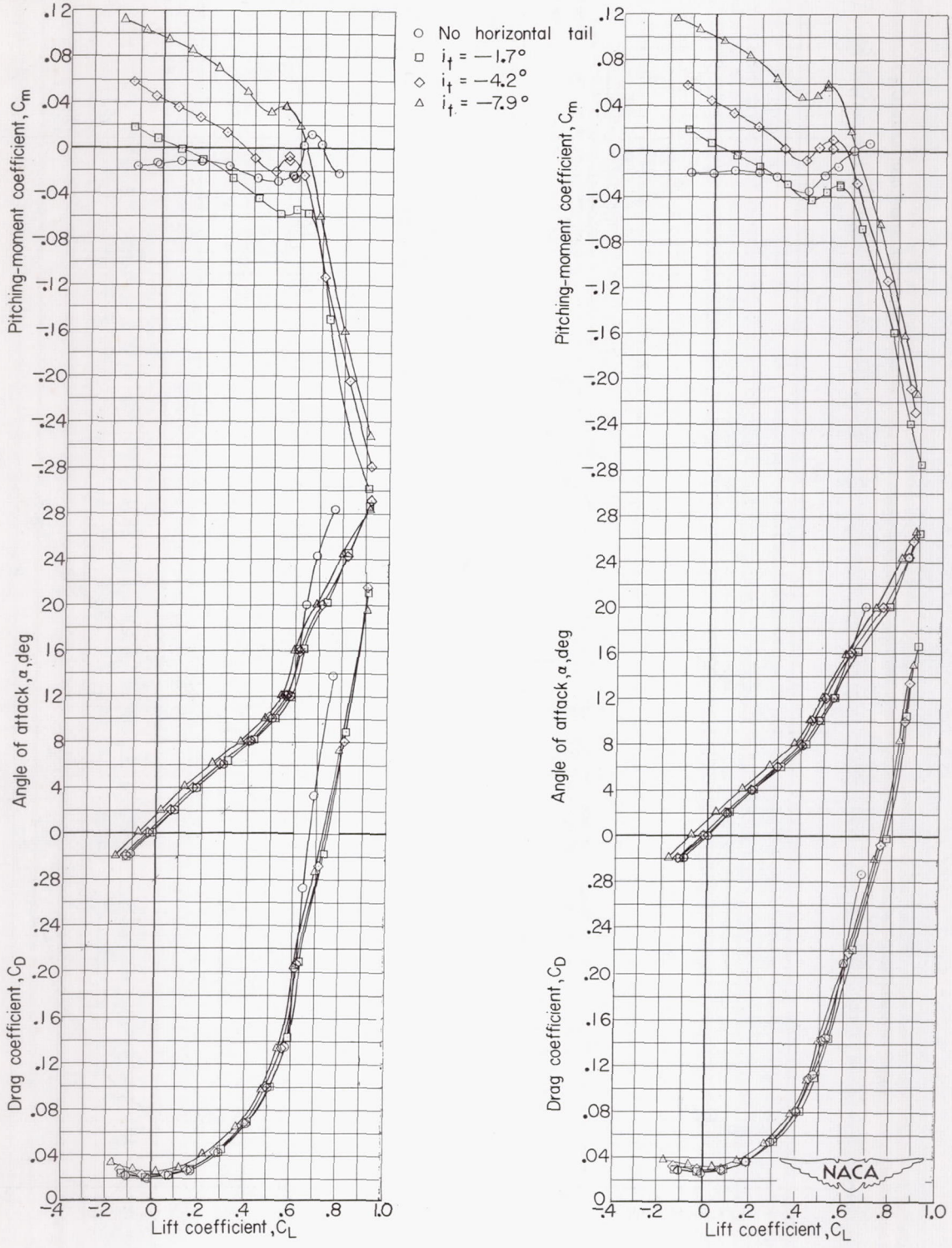
Figure 4.- The effect of stabilizer incidence on the aerodynamic characteristics of the model.



(c) M = 0.85. (d) M = 0.90.

Figure 4.- Continued.

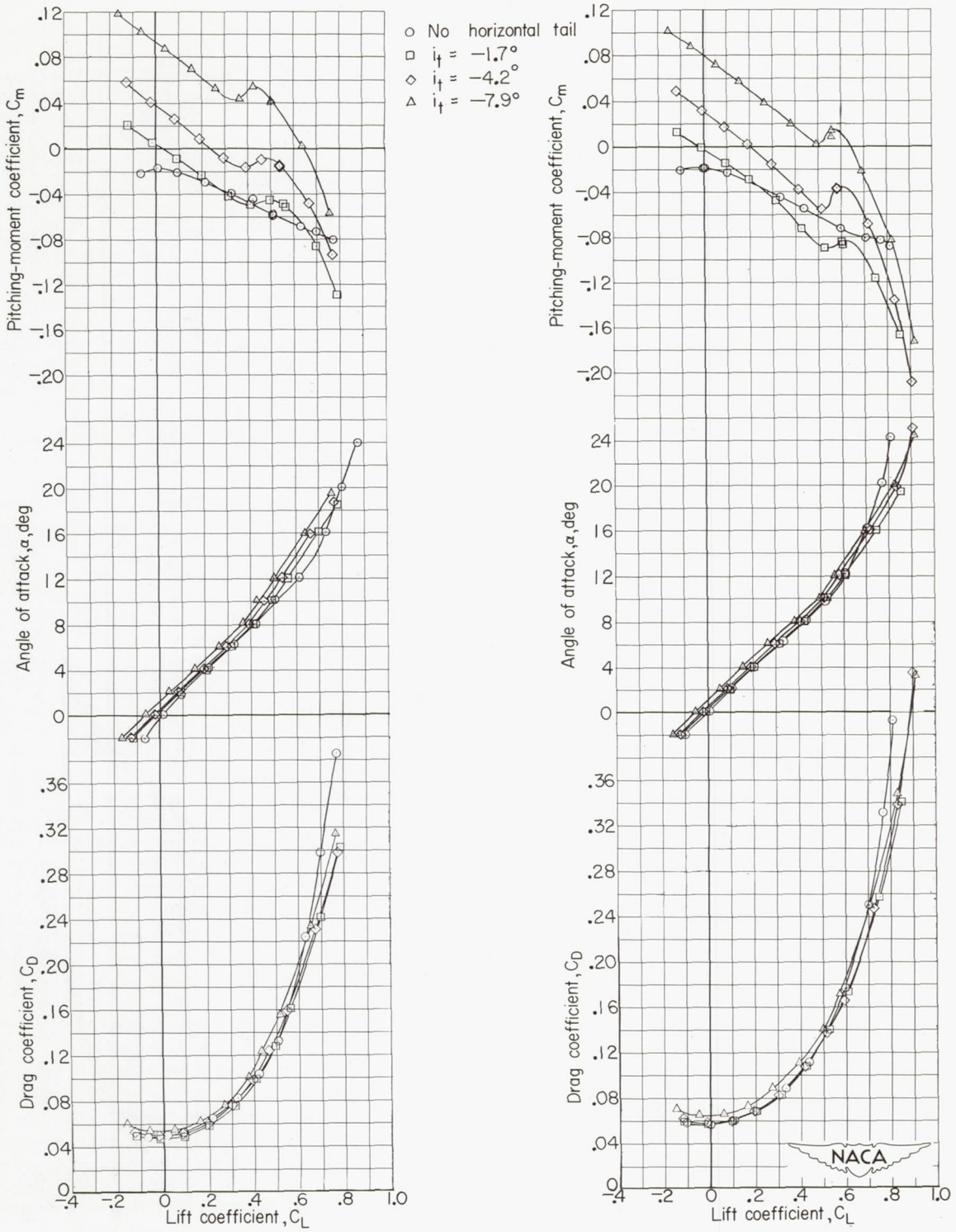
4X



(e) M = 0.93.

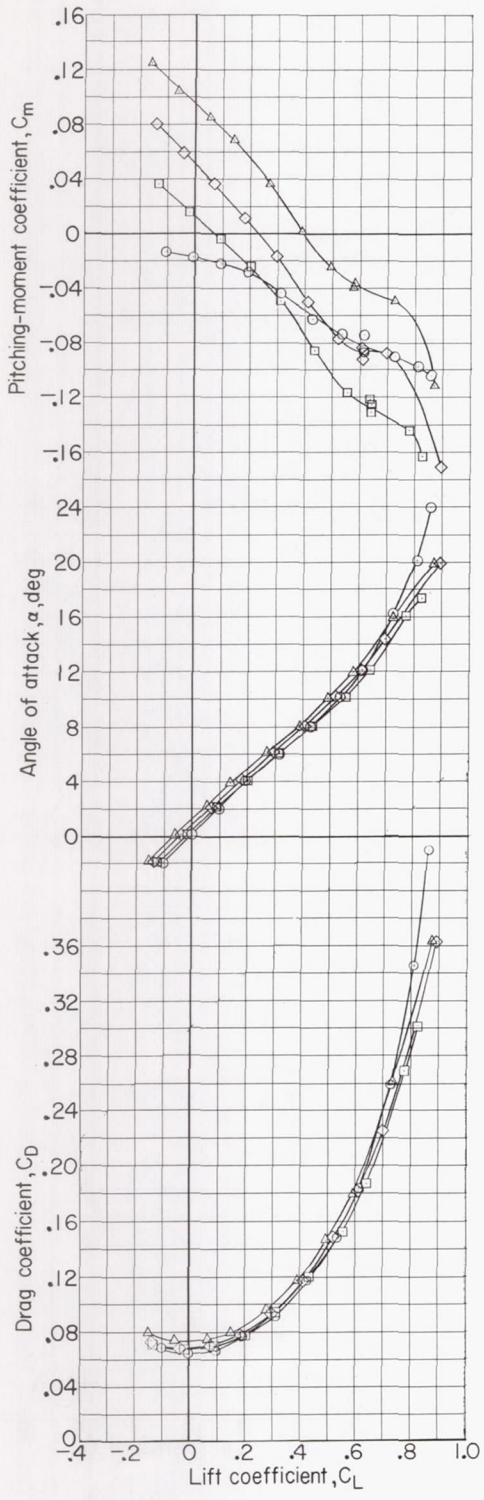
(f) M = 0.96.

Figure 4.- Continued.

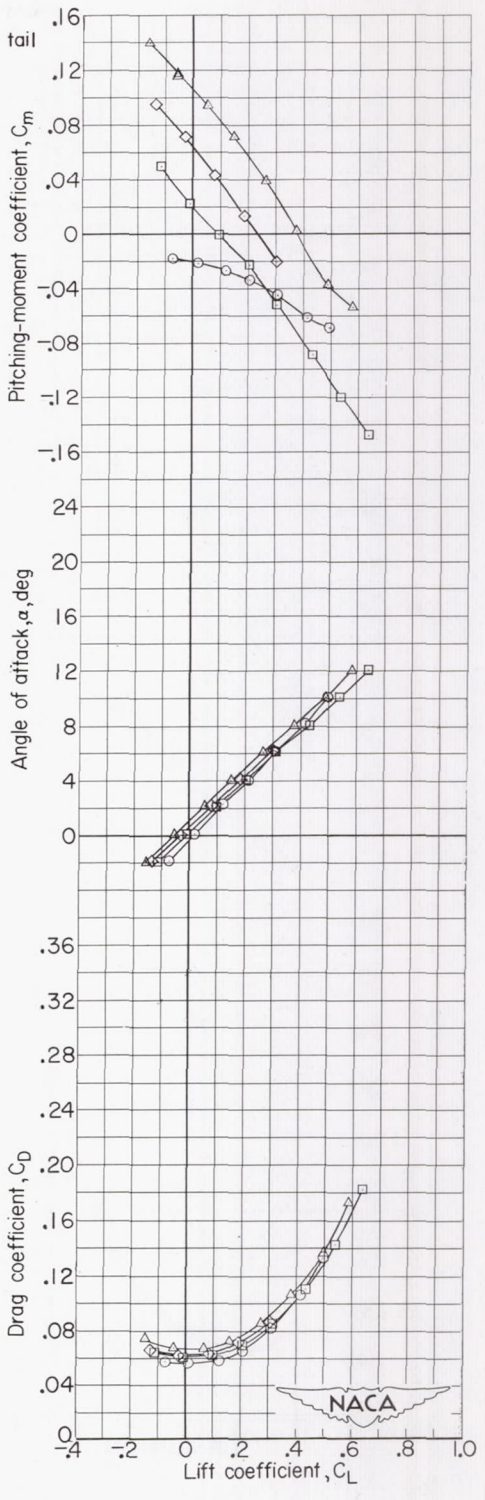


(g) M = 1.00. (h) M = 1.03.

Figure 4.- Continued.



(i) M = 1.06.



(j) M = 1.10.

Figure 4.- Concluded.

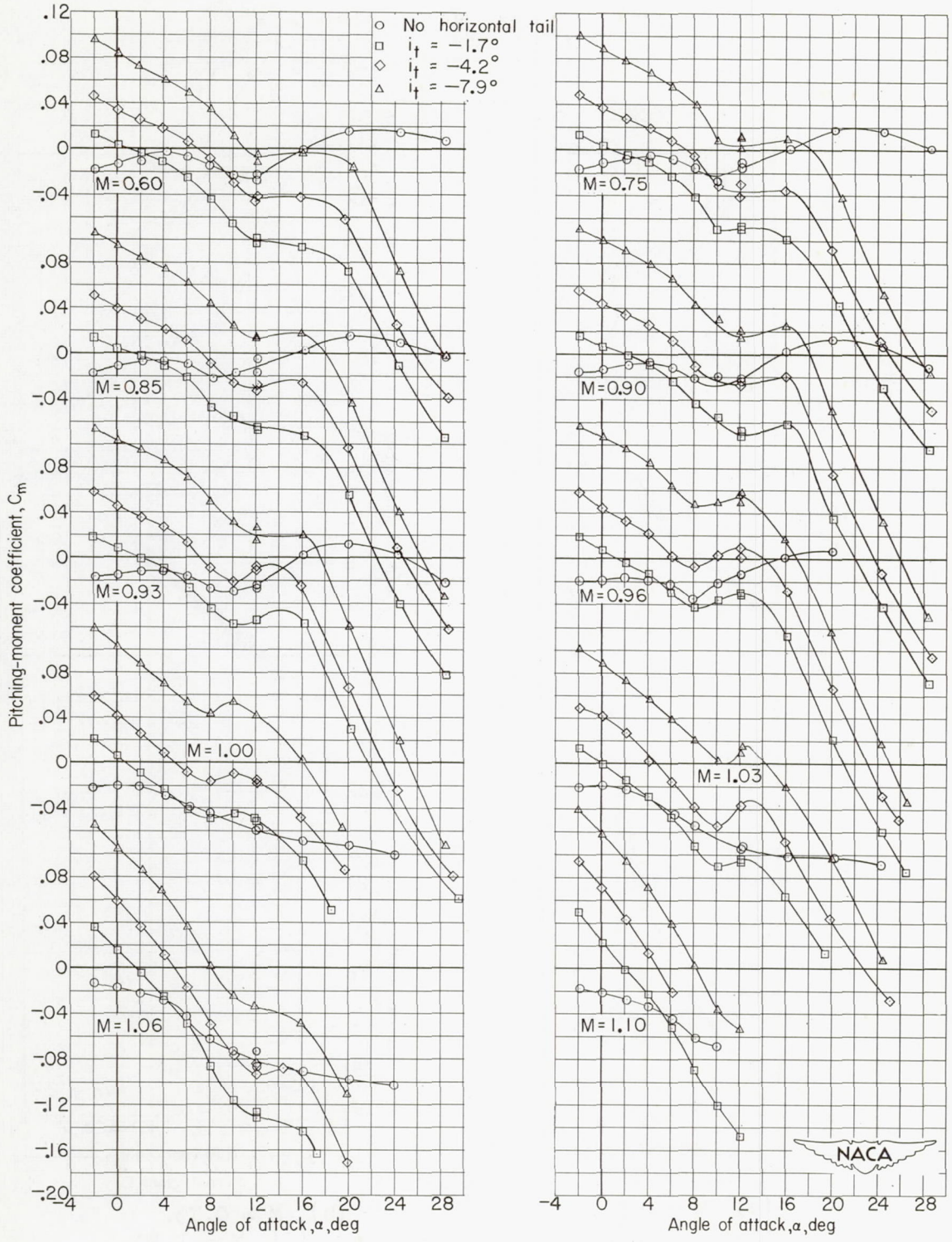
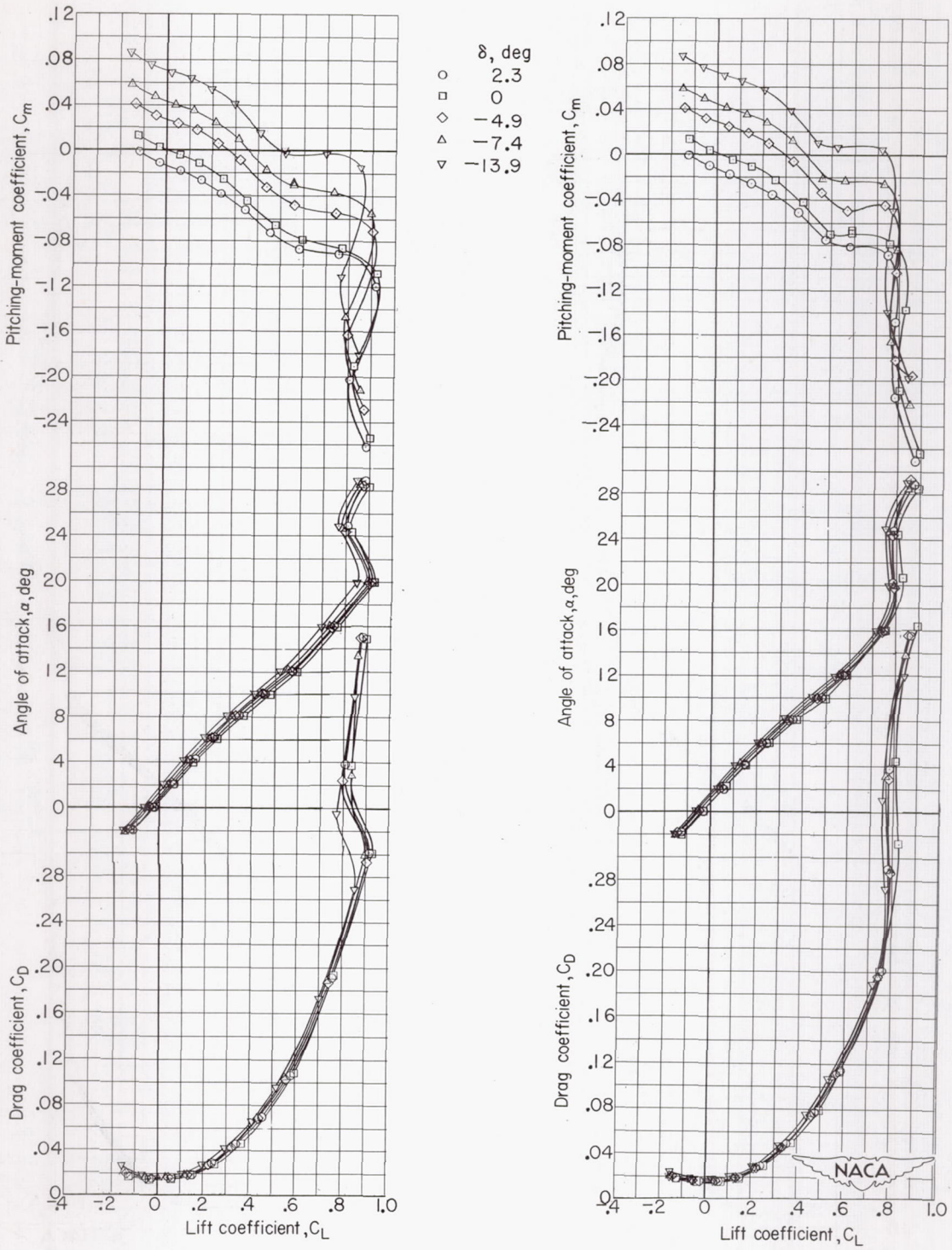
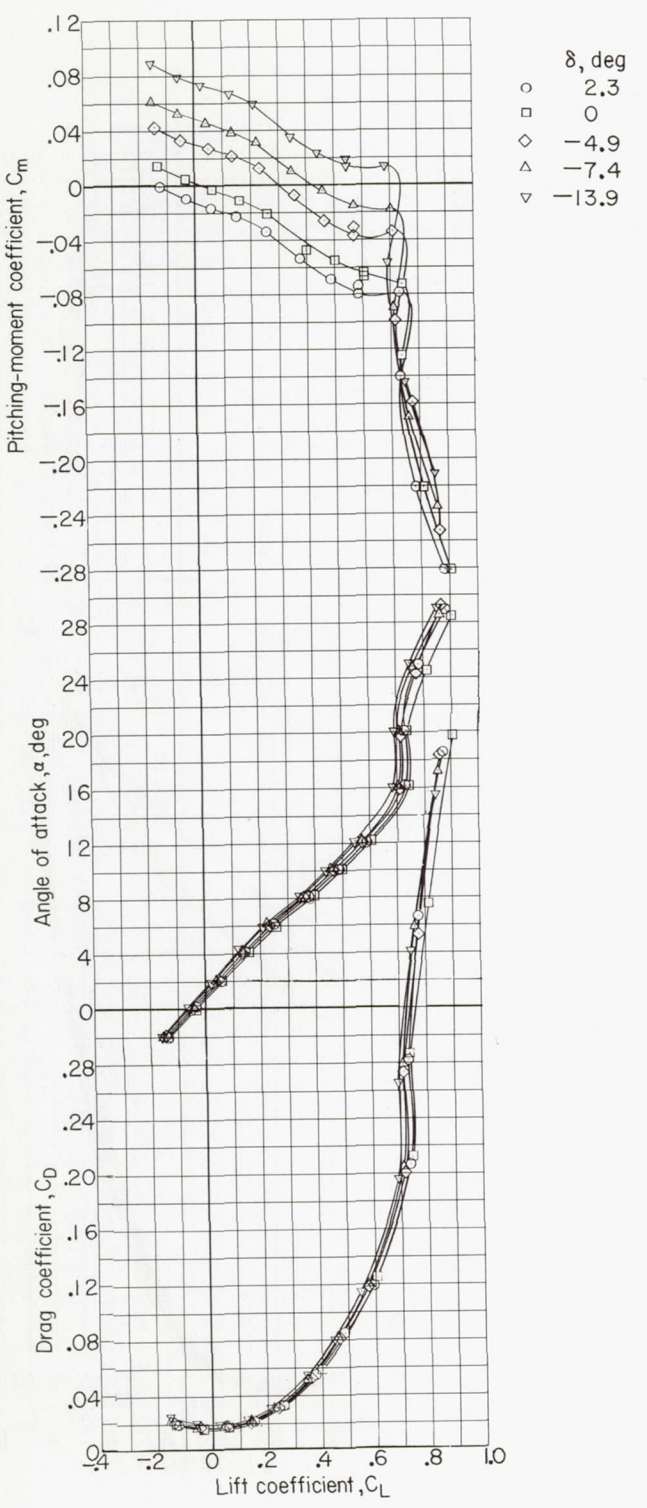


Figure 5.- The effect of stabilizer incidence on the variation of pitching-moment coefficient with angle of attack.

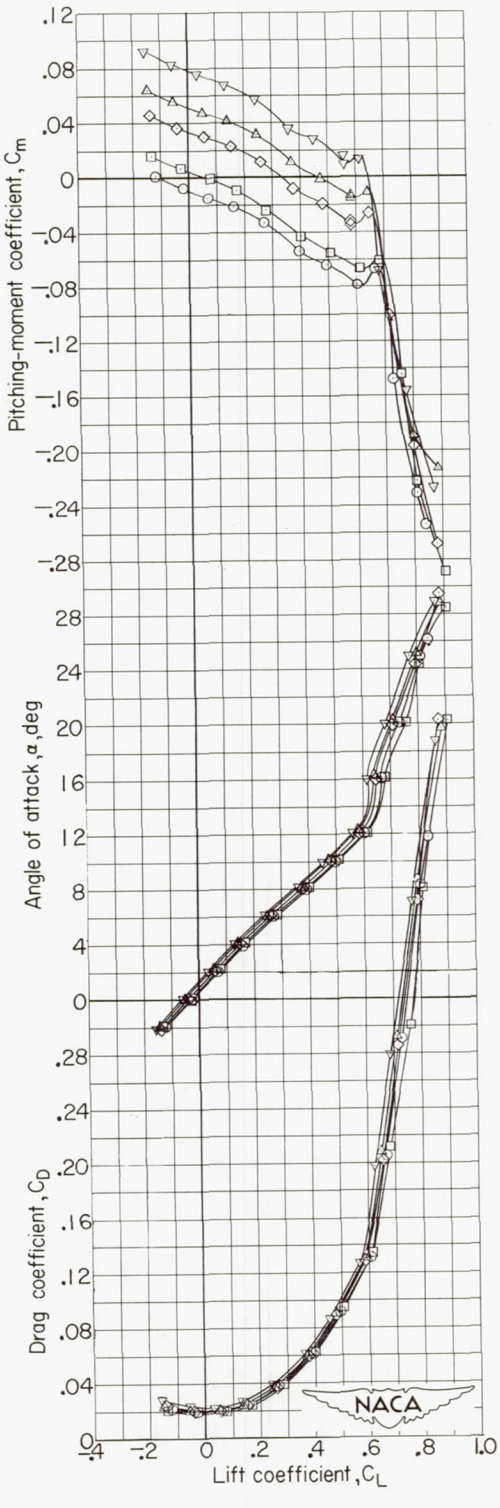


(a) M = 0.60. (b) M = 0.75.

Figure 6.- The effect of elevator deflection on the aerodynamic characteristics of the model. $i_t = -1.7^\circ$.

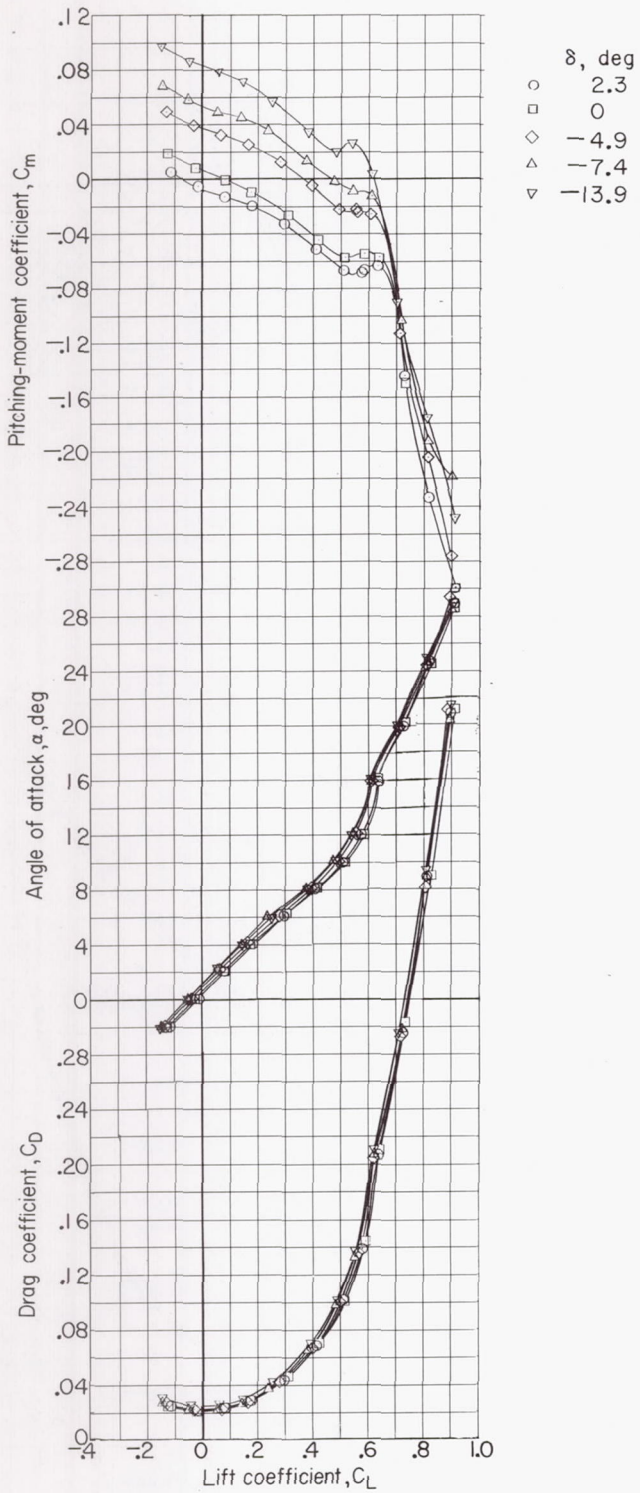


(c) M = 0.85.

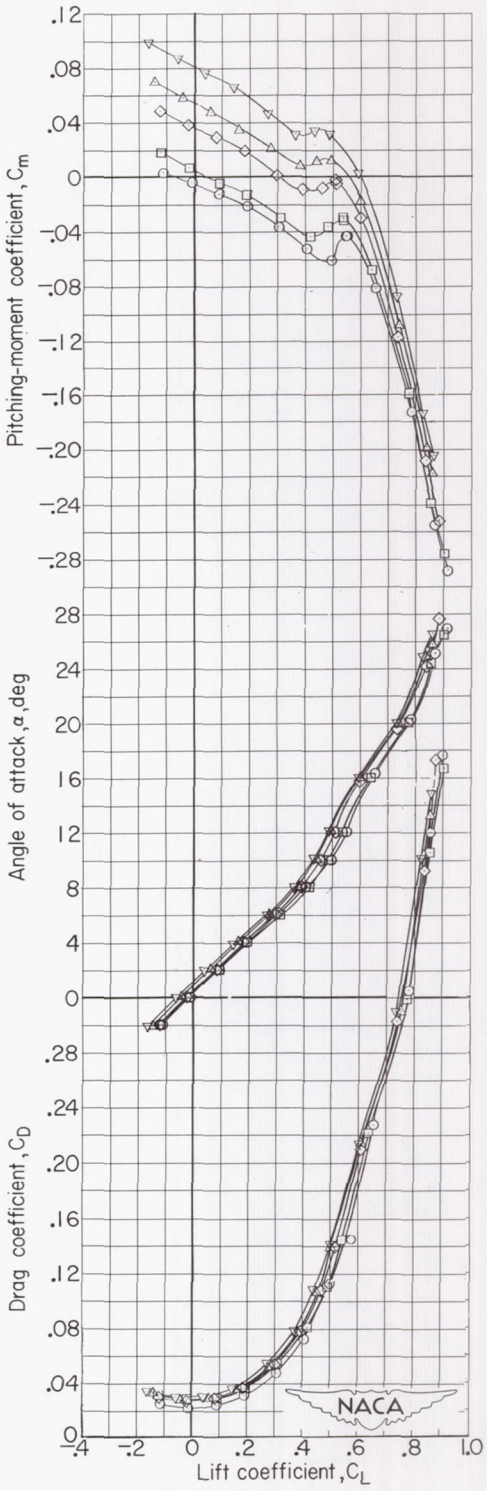


(d) M = 0.90.

Figure 6.- Continued.

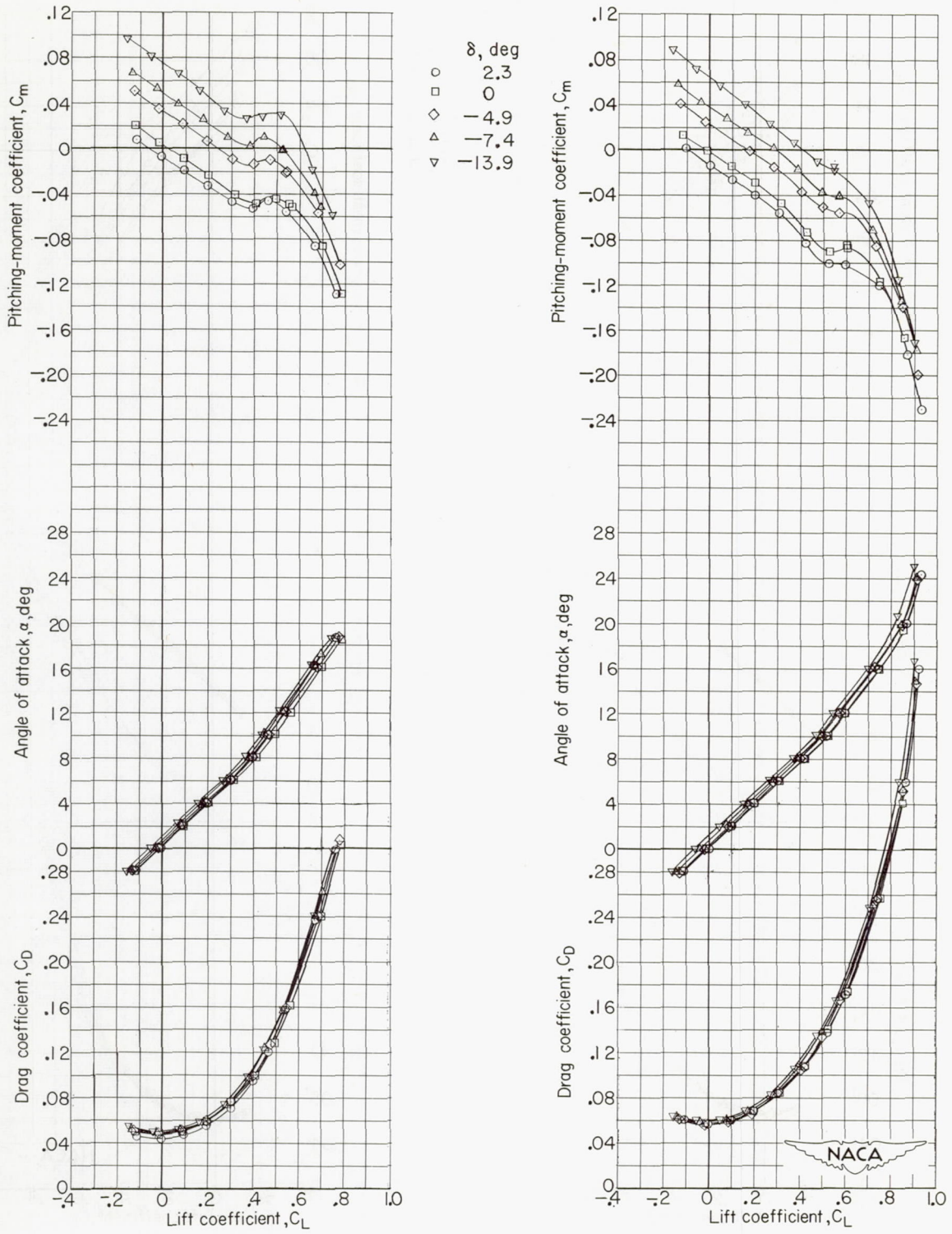


(e) M = 0.93.



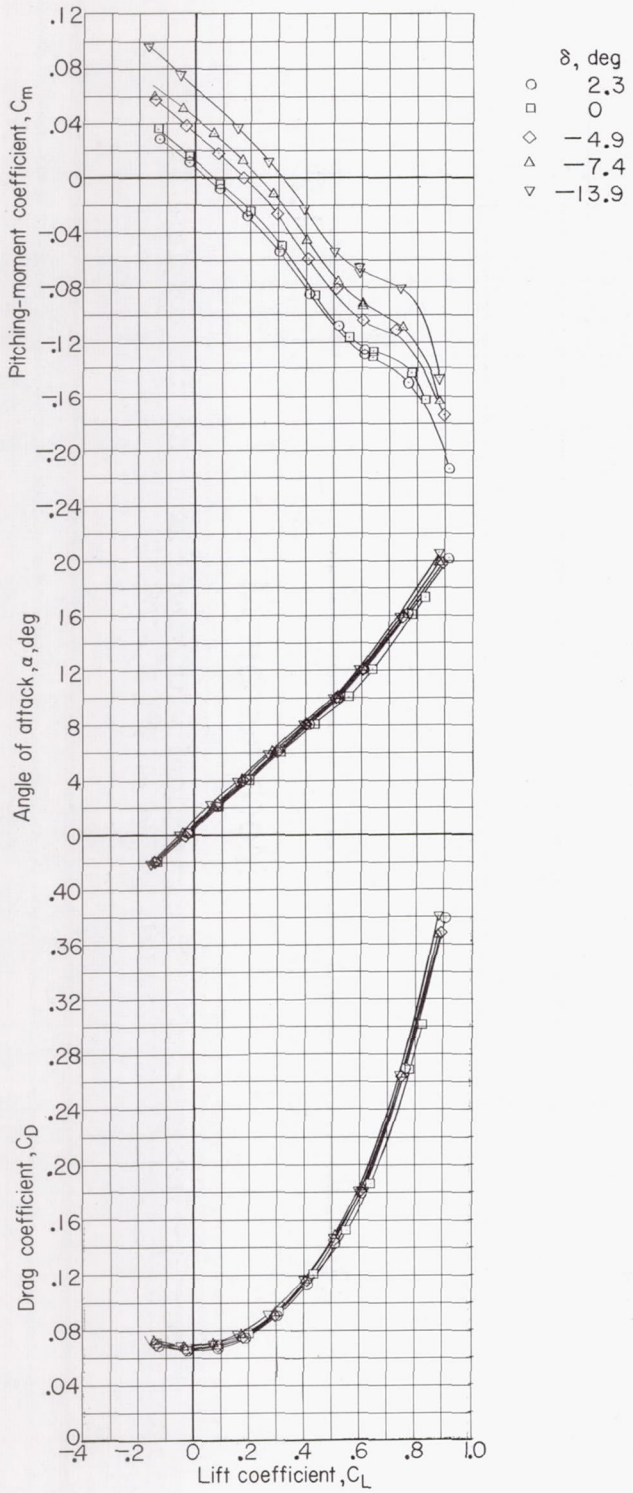
(f) M = 0.96.

Figure 6.- Continued.

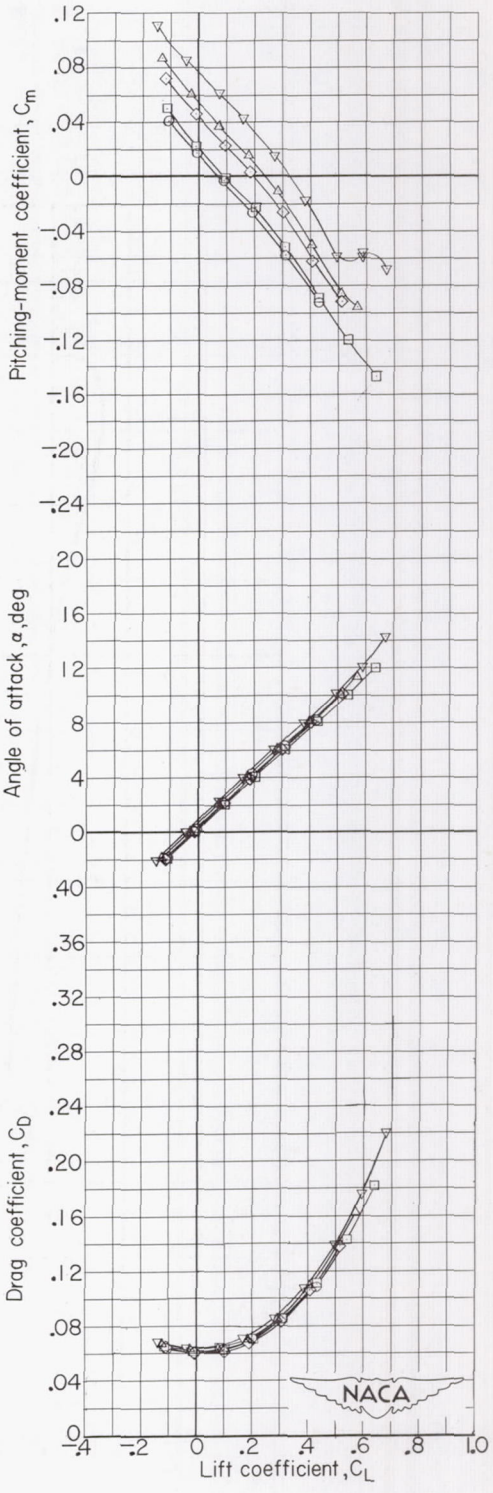


(g) M = 1.00. (h) M = 1.03.

Figure 6.- Continued.



(i) M = 1.06.



(j) M = 1.10.

Figure 6.- Concluded.

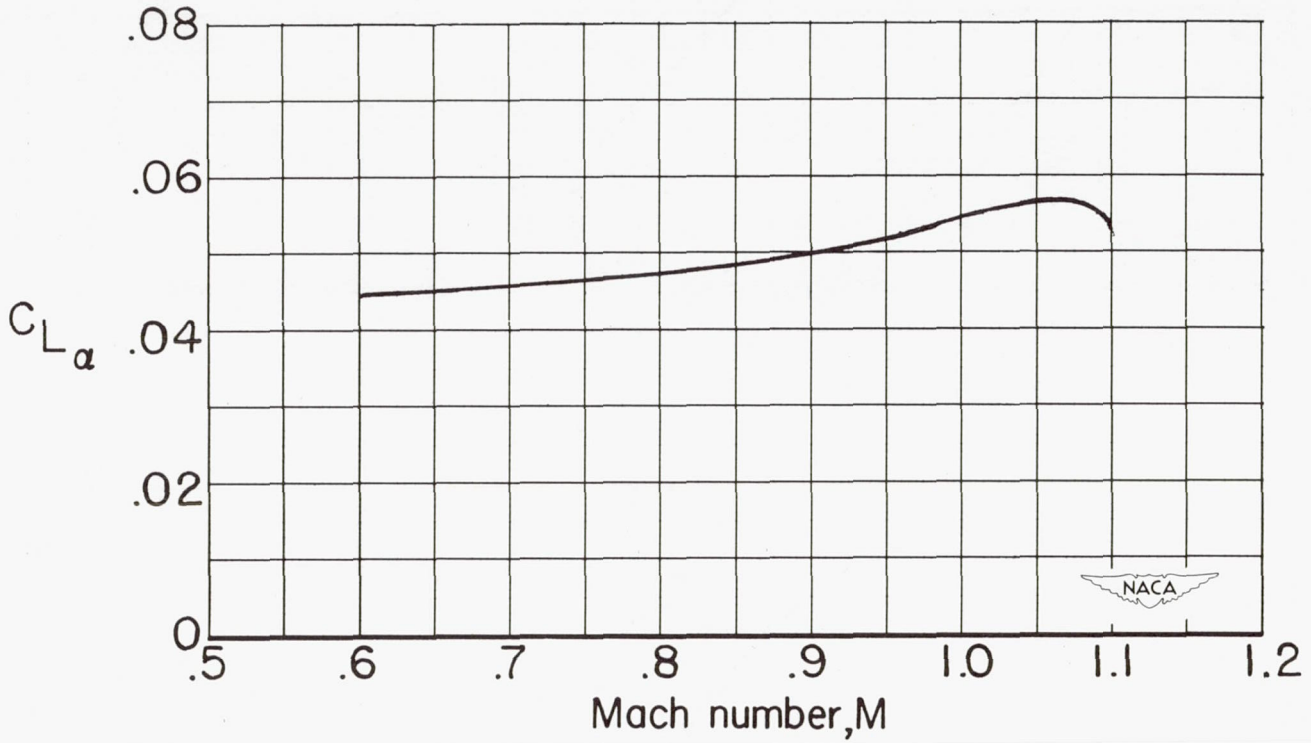
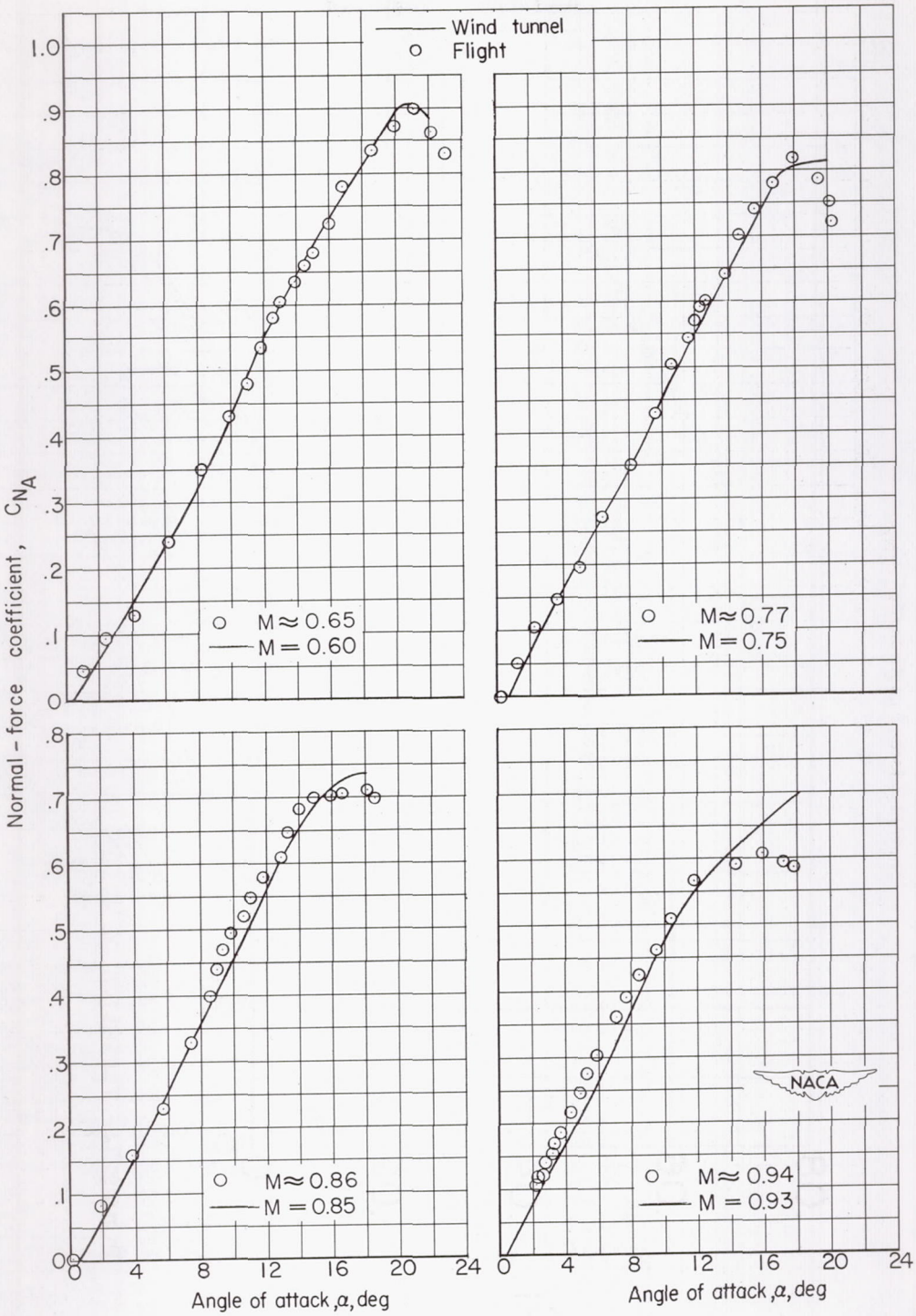
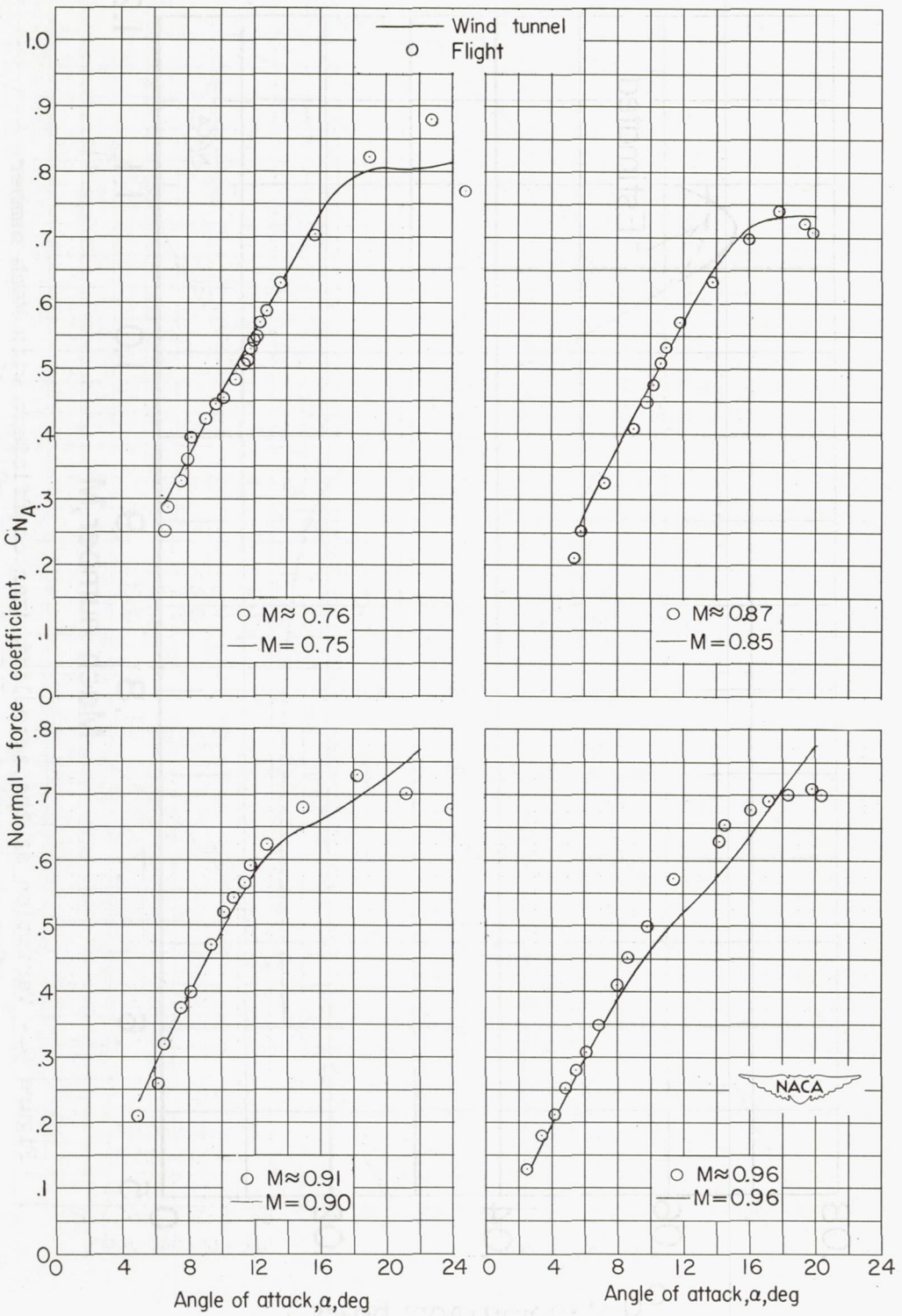


Figure 7.- Variation of lift-curve slope with Mach number for the complete model. $i_t = -1.7^\circ$; $\delta = 0^\circ$.



(a) Elevator maneuver.

Figure 8.- Variation of normal-force coefficient with angle of attack; comparison of flight and wind-tunnel data.



(b) Stabilizer maneuver.

Figure 8.- Concluded.



Figure 9.- Variation of the zero-lift drag coefficient with Mach number for the complete model. $i_t = -1.7^\circ$; $\delta = 0^\circ$.

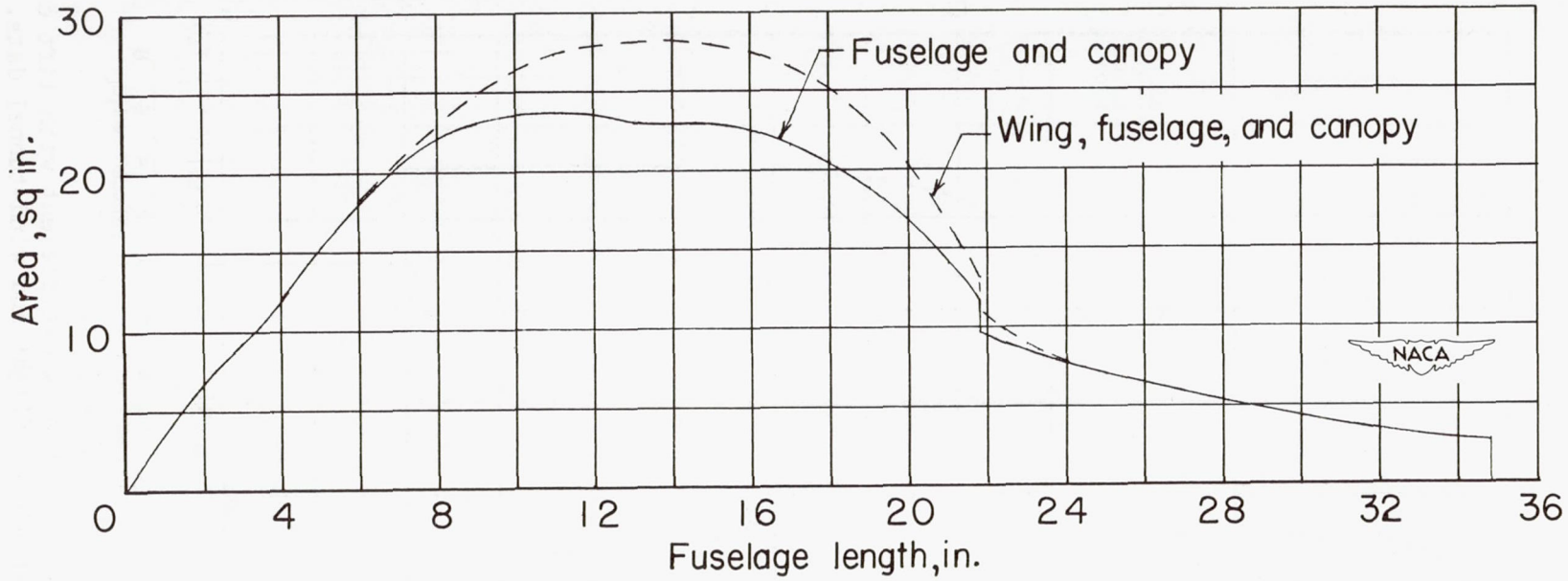


Figure 10.- Axial distribution of cross-sectional area of the model.

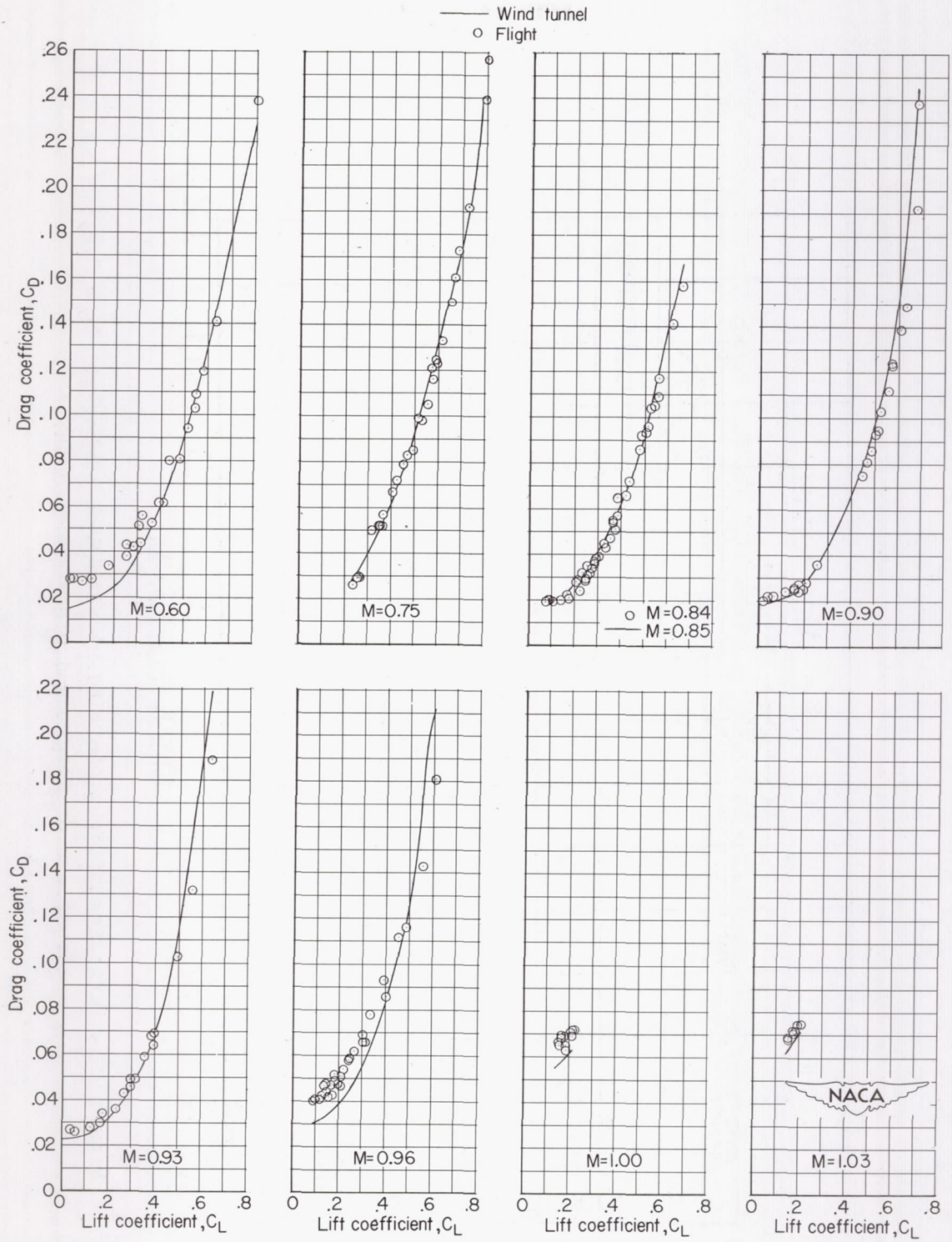


Figure 11.- Variation of drag coefficient with lift coefficient; comparison of flight and wind-tunnel data.

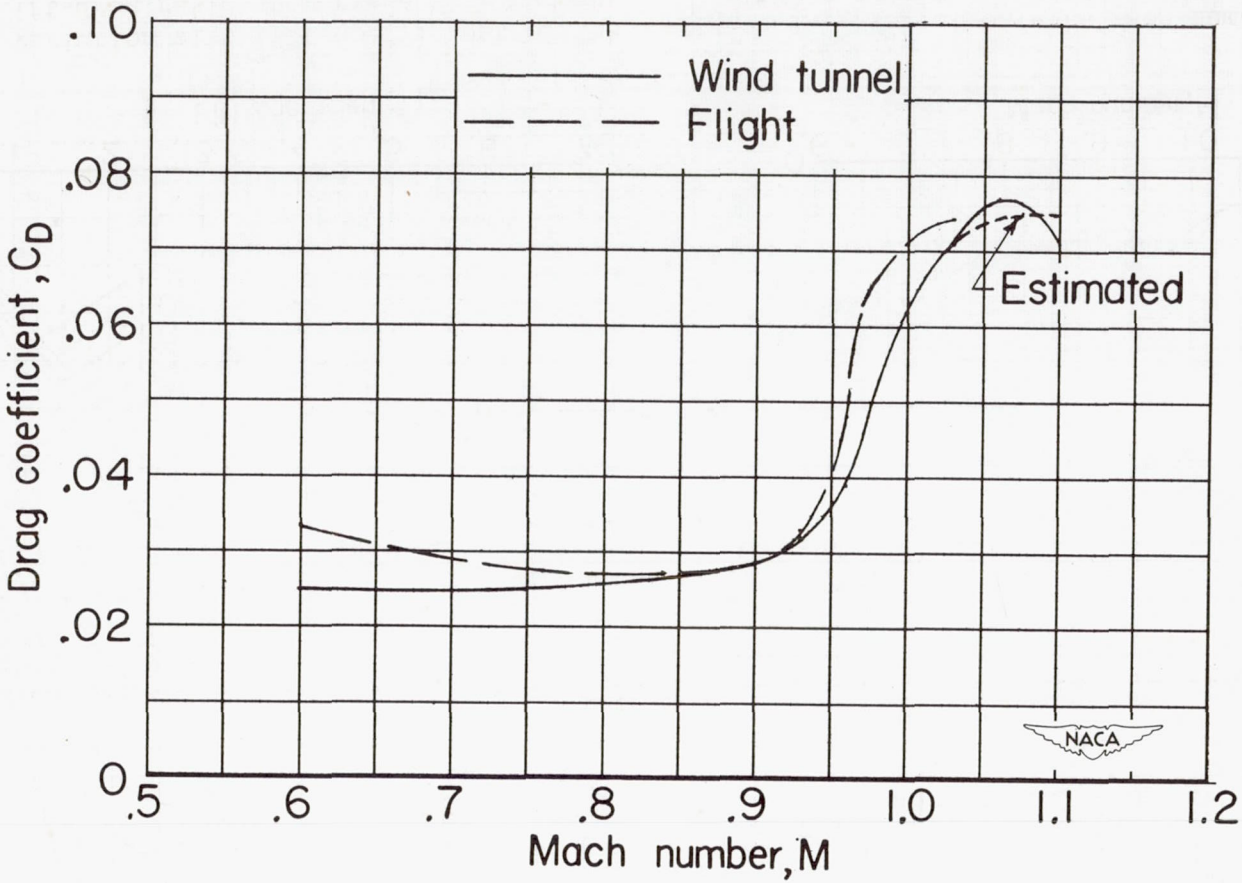


Figure 12.- Variation of drag coefficient with Mach number at $C_L = 0.2$; comparison of flight and wind-tunnel data.

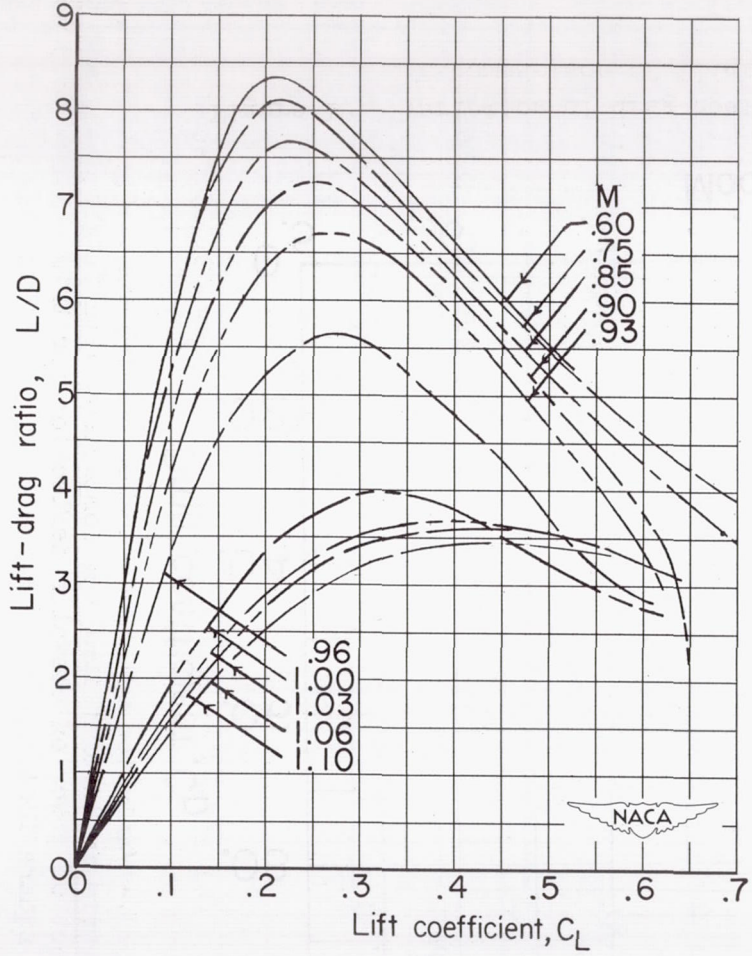


Figure 13.- Variation with lift coefficient of the trimmed lift-drag ratio at various Mach numbers.

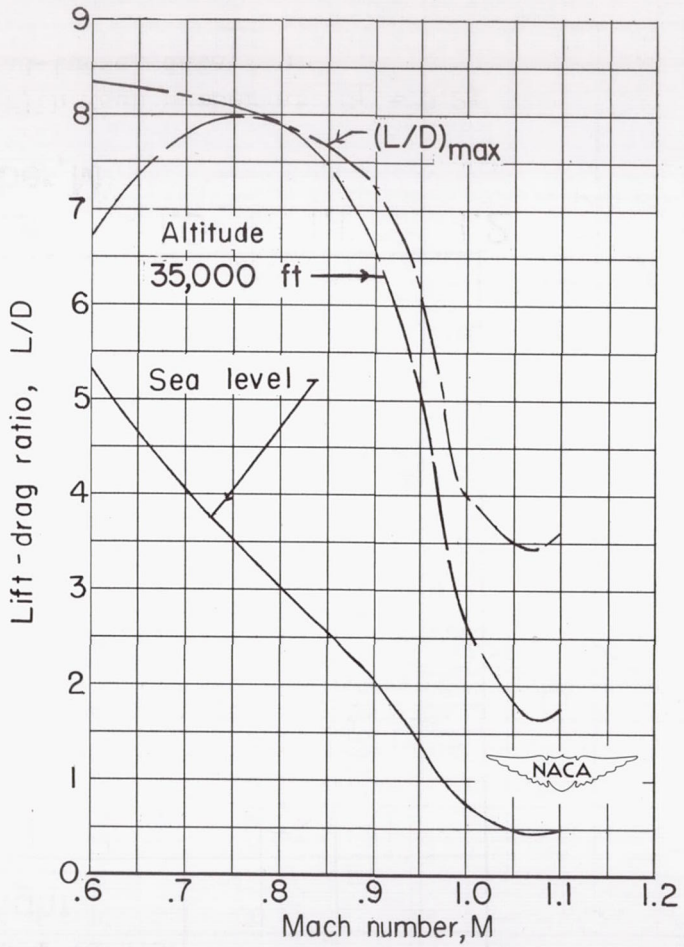
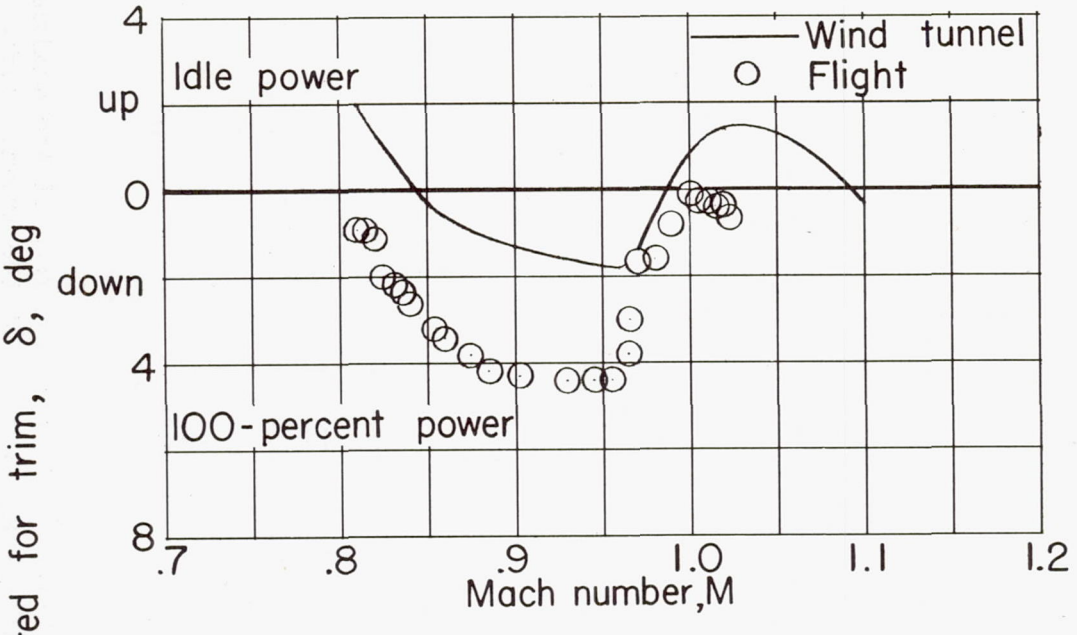
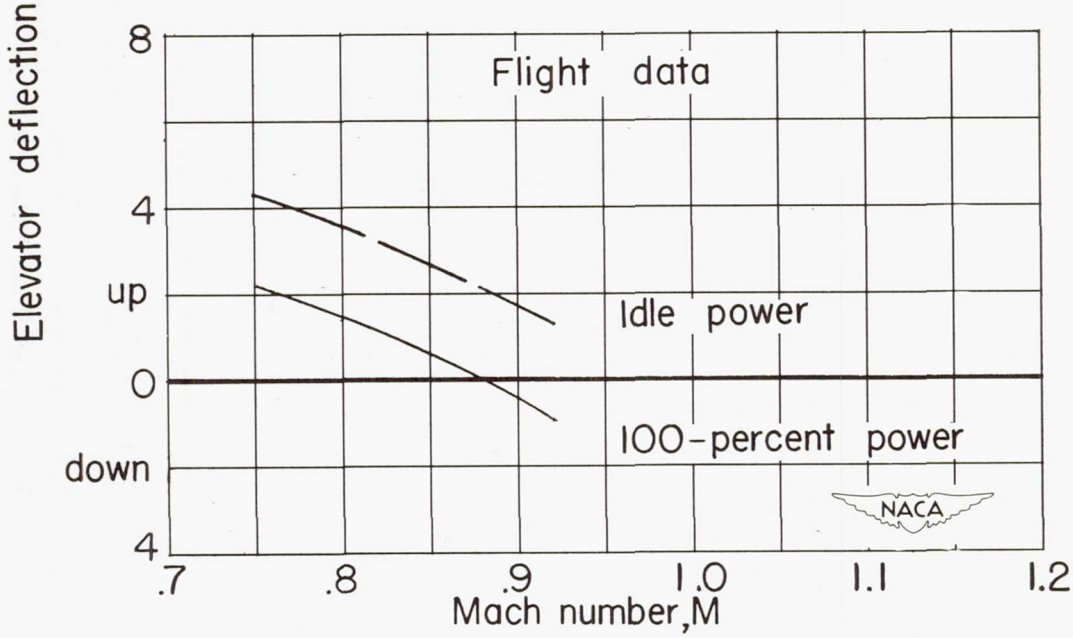


Figure 14.- Variation with Mach number of the maximum trimmed lift-drag ratio and of the trimmed lift-drag ratio in level flight for sea level and 35,000 feet altitude for W/S = 48.5 pounds per square foot.



(a) Elevator deflection required for trim. $i_t = -2.6^\circ$; $h_p = 42{,}000$ feet.



(b) Effect of power. $i_t = -2.1^\circ$; $h_p = 40{,}000$ feet.

Figure 15.- Variation with Mach number of elevator deflection required for trim in level flight and comparison with flight data, and the effect of power on elevator deflection for trim. W/S = 48.5 pounds per square foot.

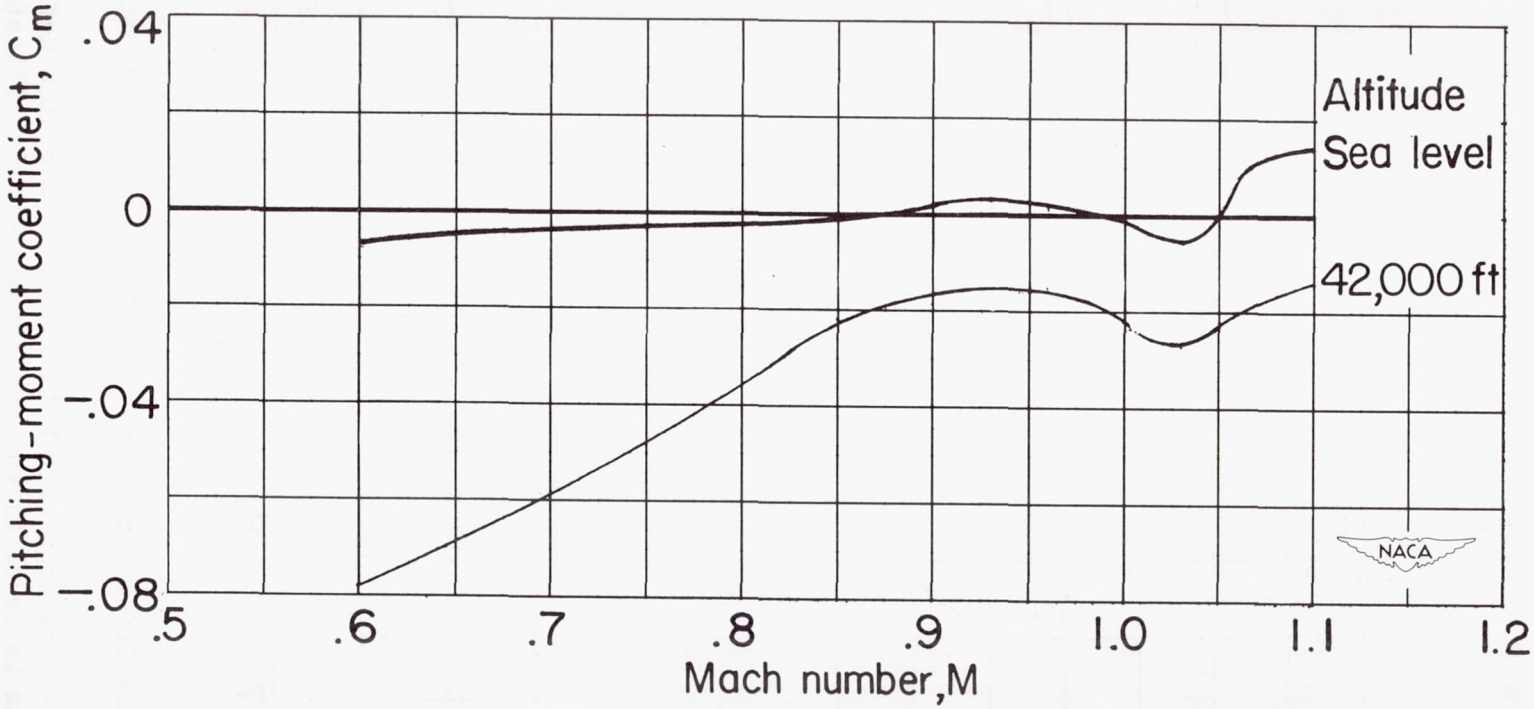


Figure 16.- Variation with Mach number of the out-of-trim pitching-moment coefficient of the model. W/S = 48.5 pounds per square foot; $i_t = -1.7^\circ$; $\delta = 0^\circ$.

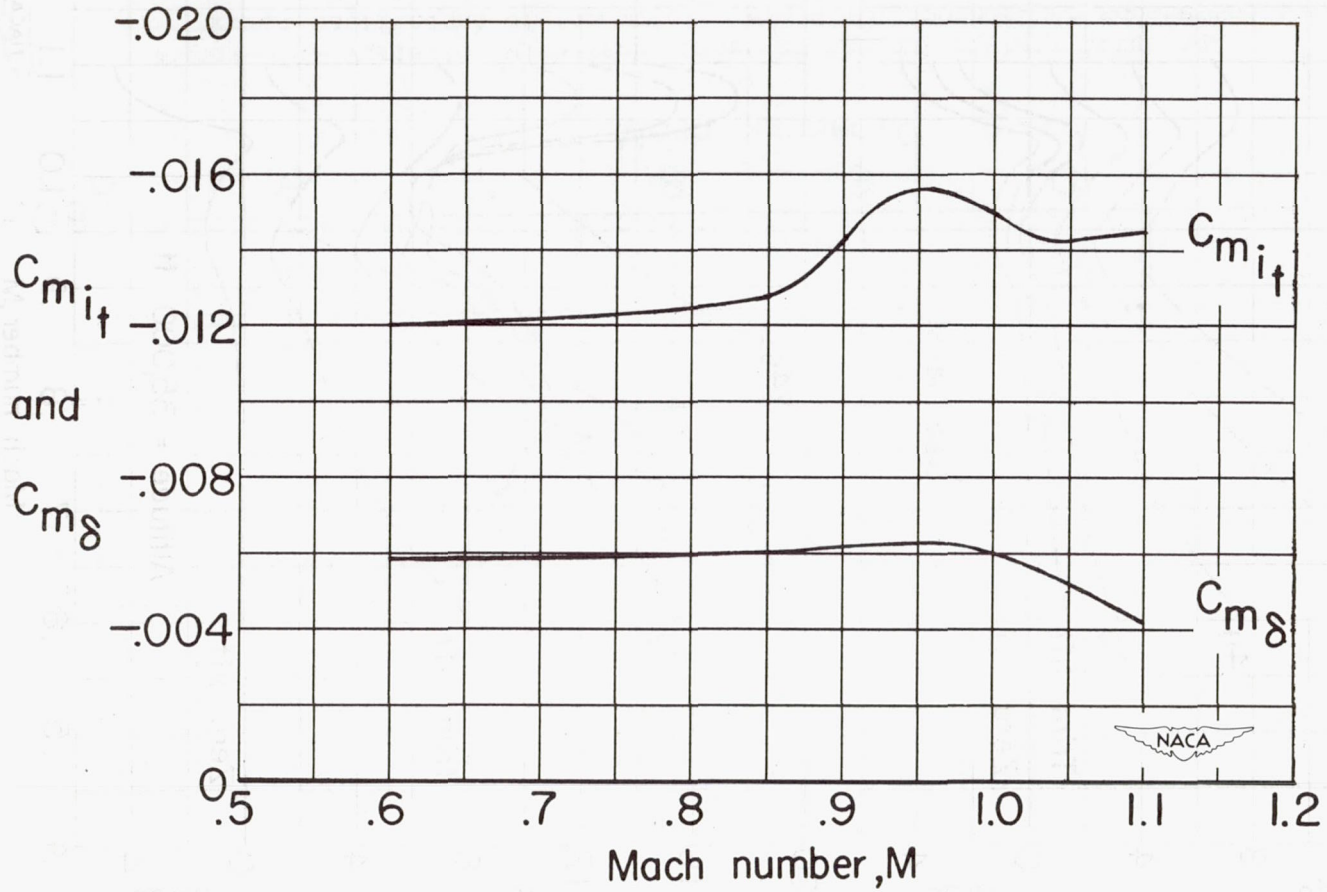


Figure 17.- Variation with Mach number of the stabilizer and elevator effectiveness parameters.

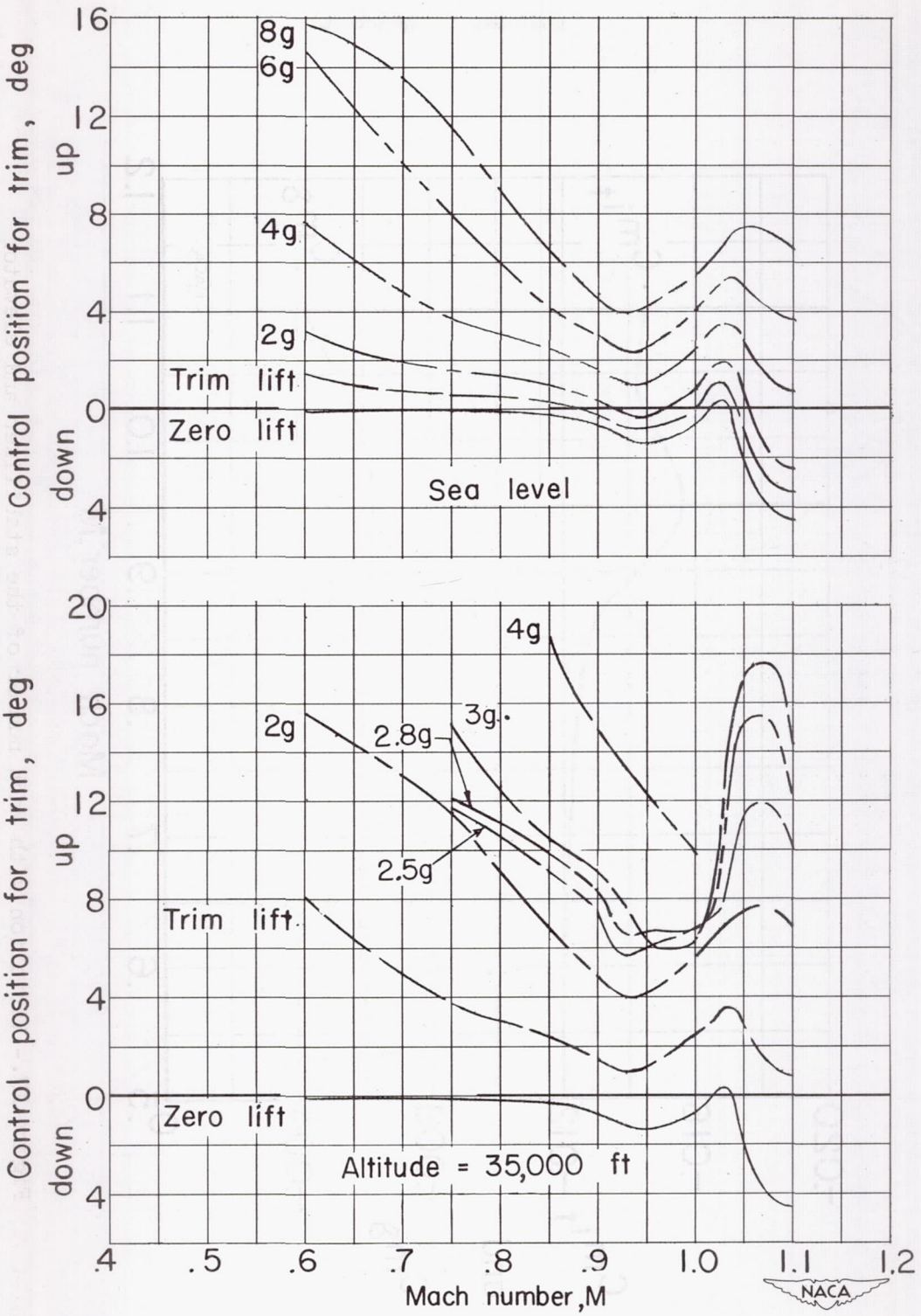


Figure 18.- Variation with Mach number of elevator control position required for trim in level and accelerated flight at sea level and 35,000 feet altitude. W/S = 48.5 pounds per square foot; i_t = -1.7°.

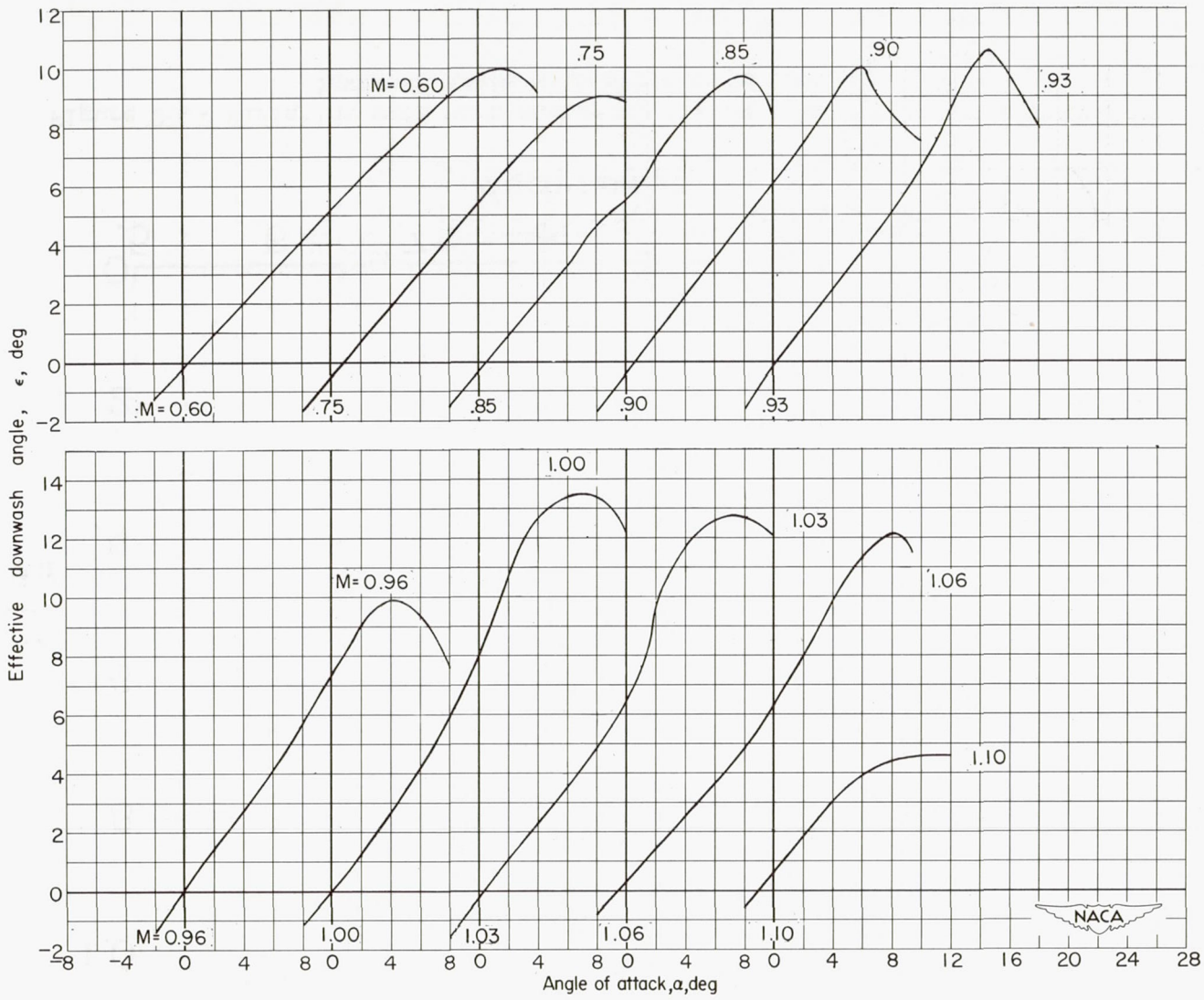


Figure 19.- Variation of the effective downwash angle with angle of attack.

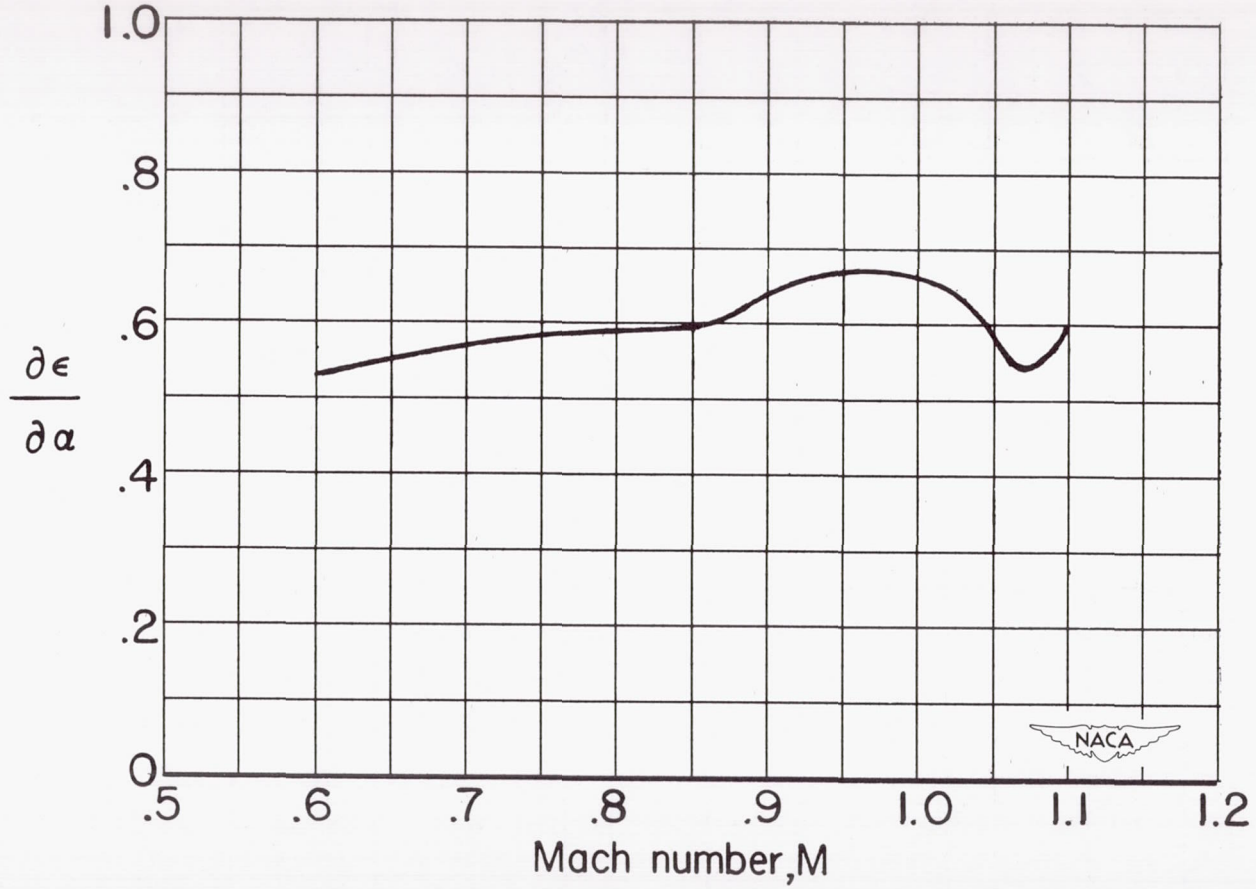
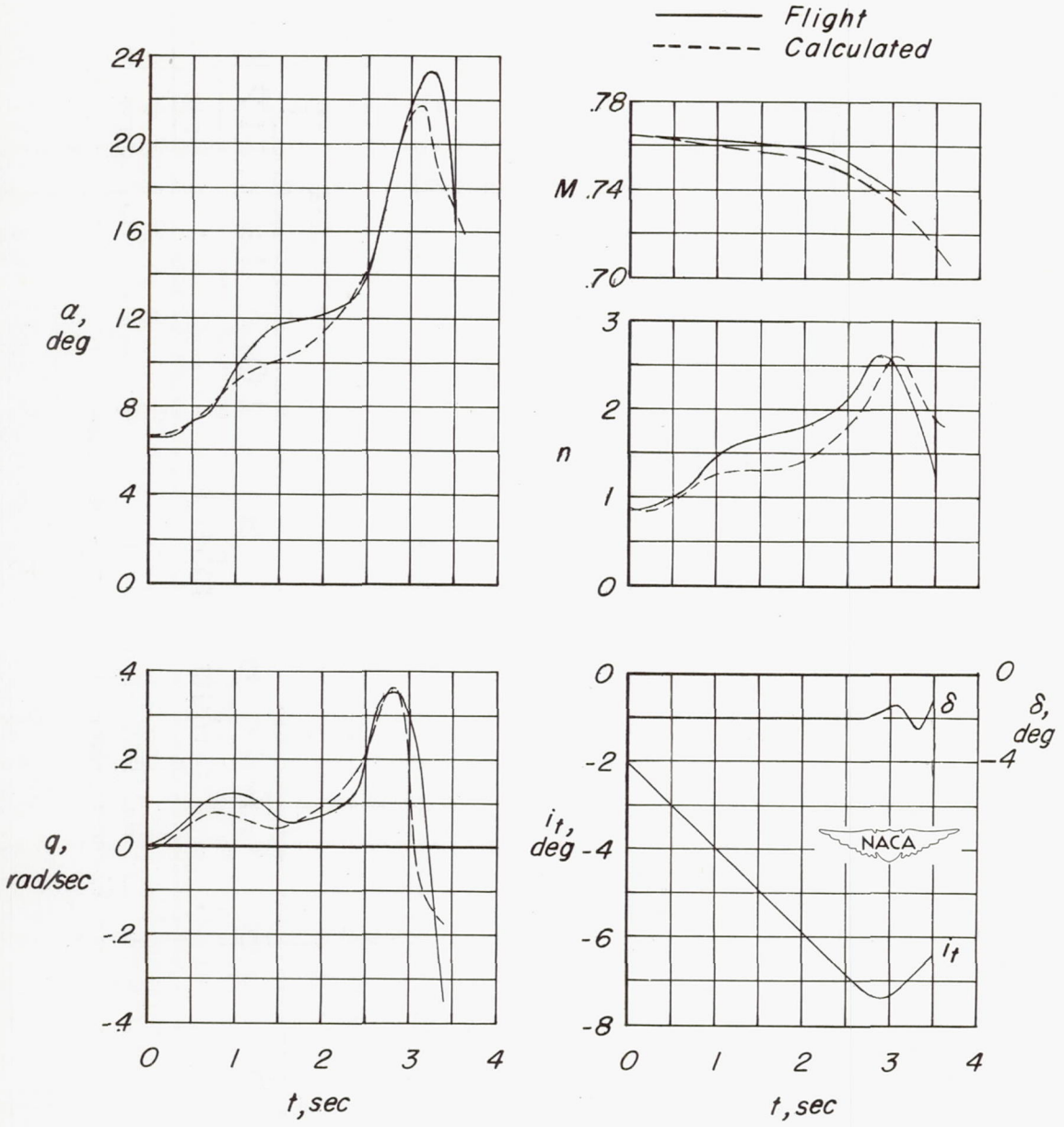
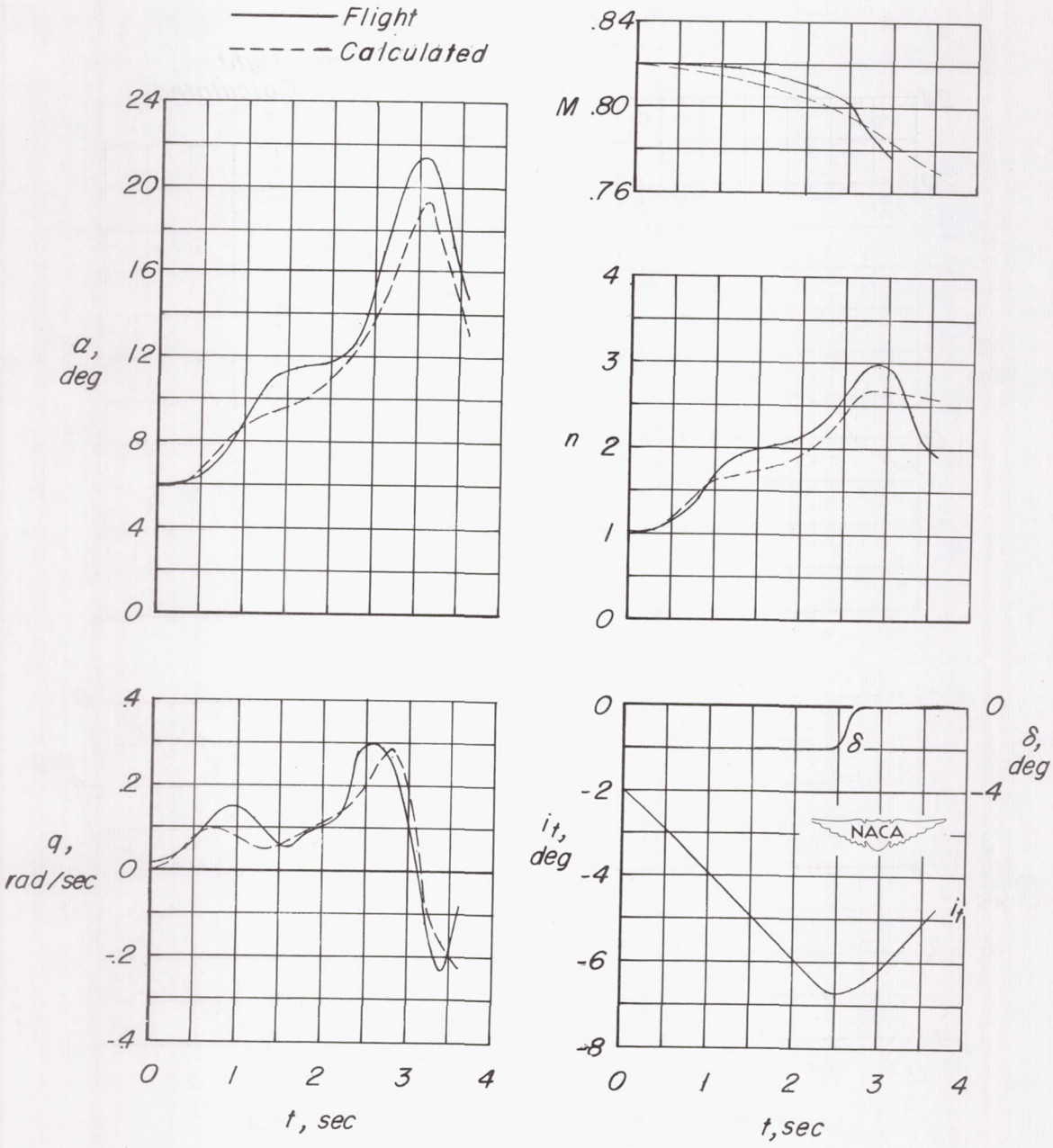


Figure 20.- Variation with Mach number of the rate of change of effective downwash angle with angle of attack.



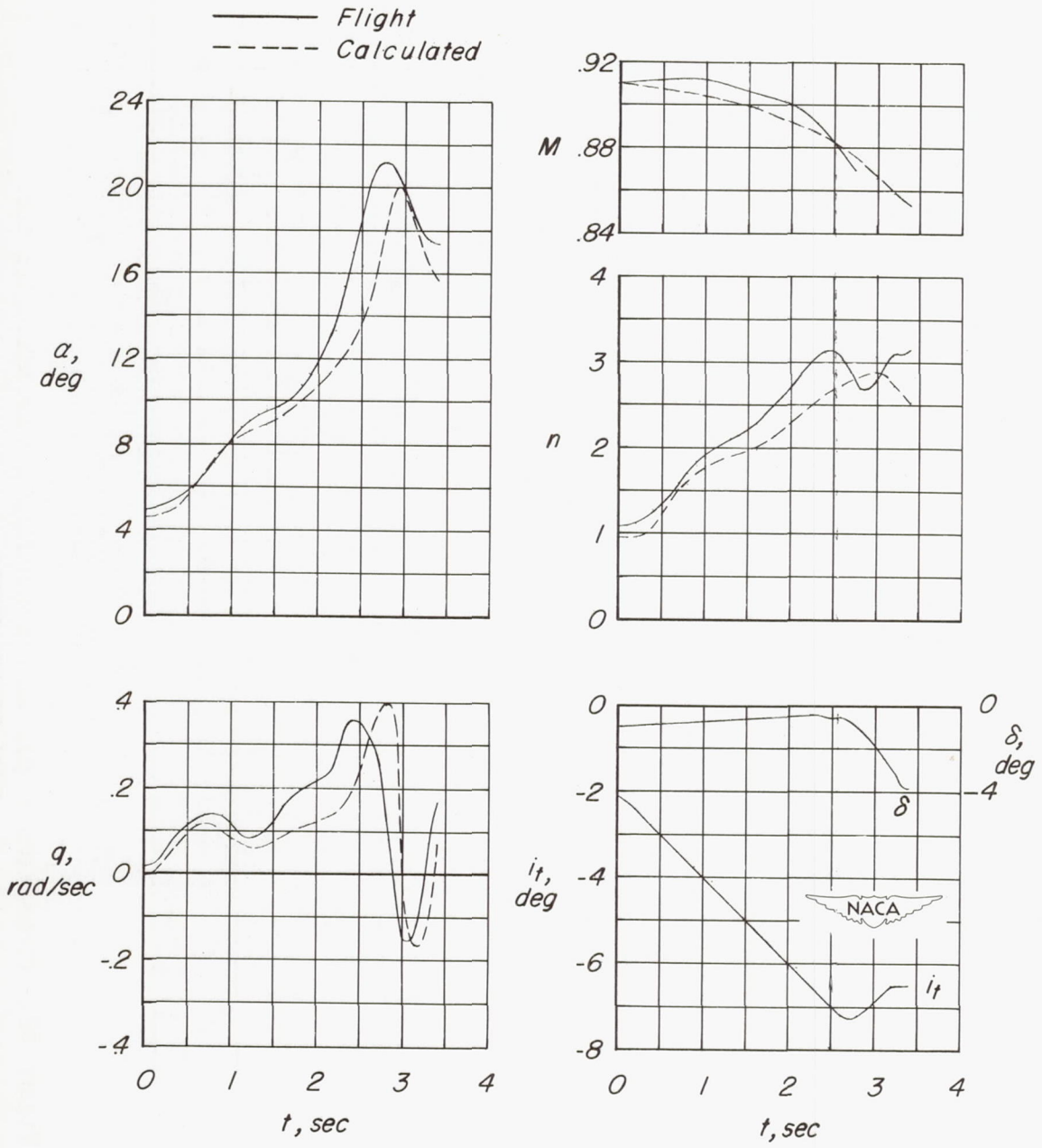
(a) $M_0 = 0.76$; $h_p = 42{,}000$ ft.

Figure 21.- Comparison of calculated and flight time histories for stabilizer pull-ups.



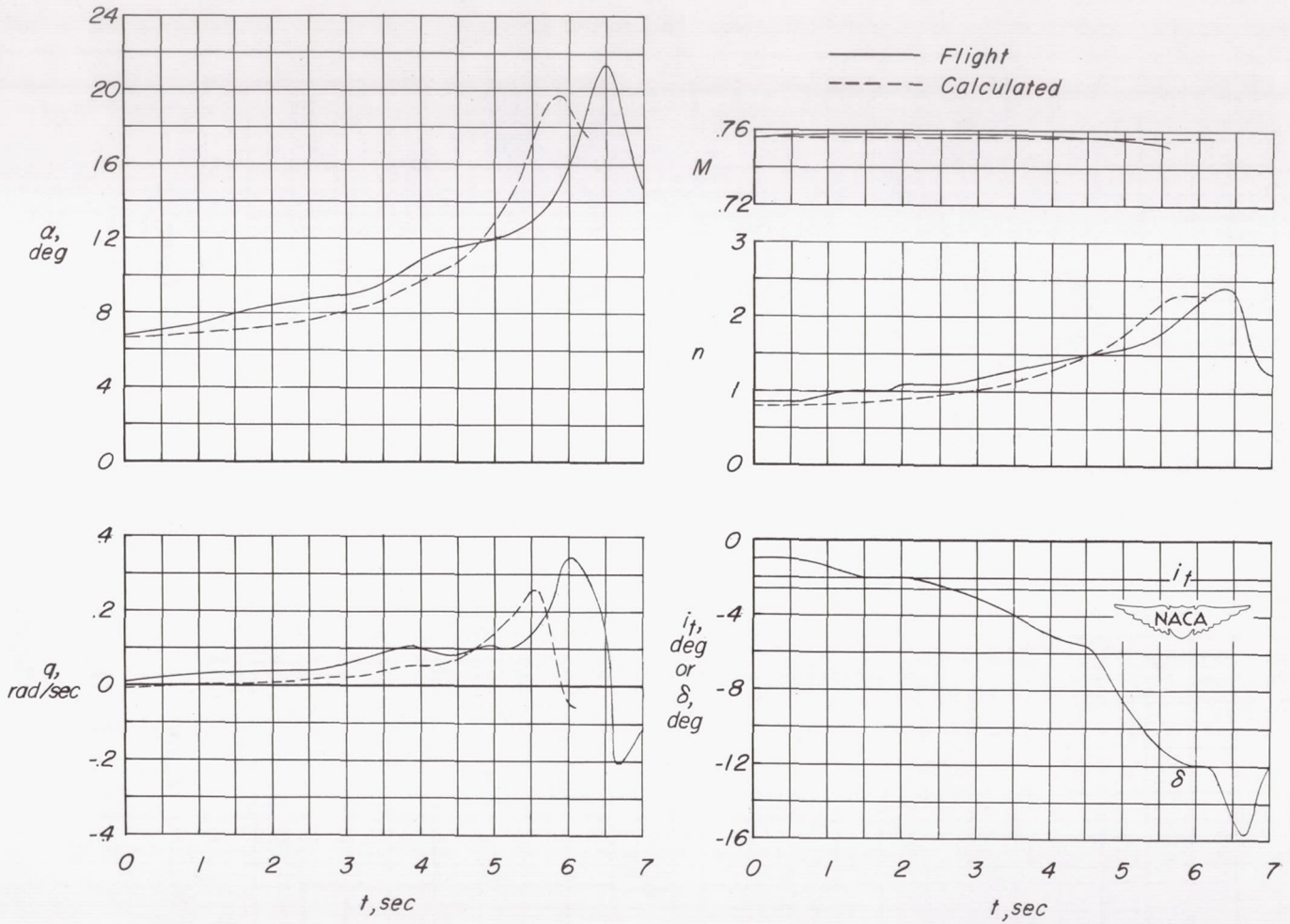
(b) M = 0.82; h_p = 39,500 ft.

Figure 21.- Continued.



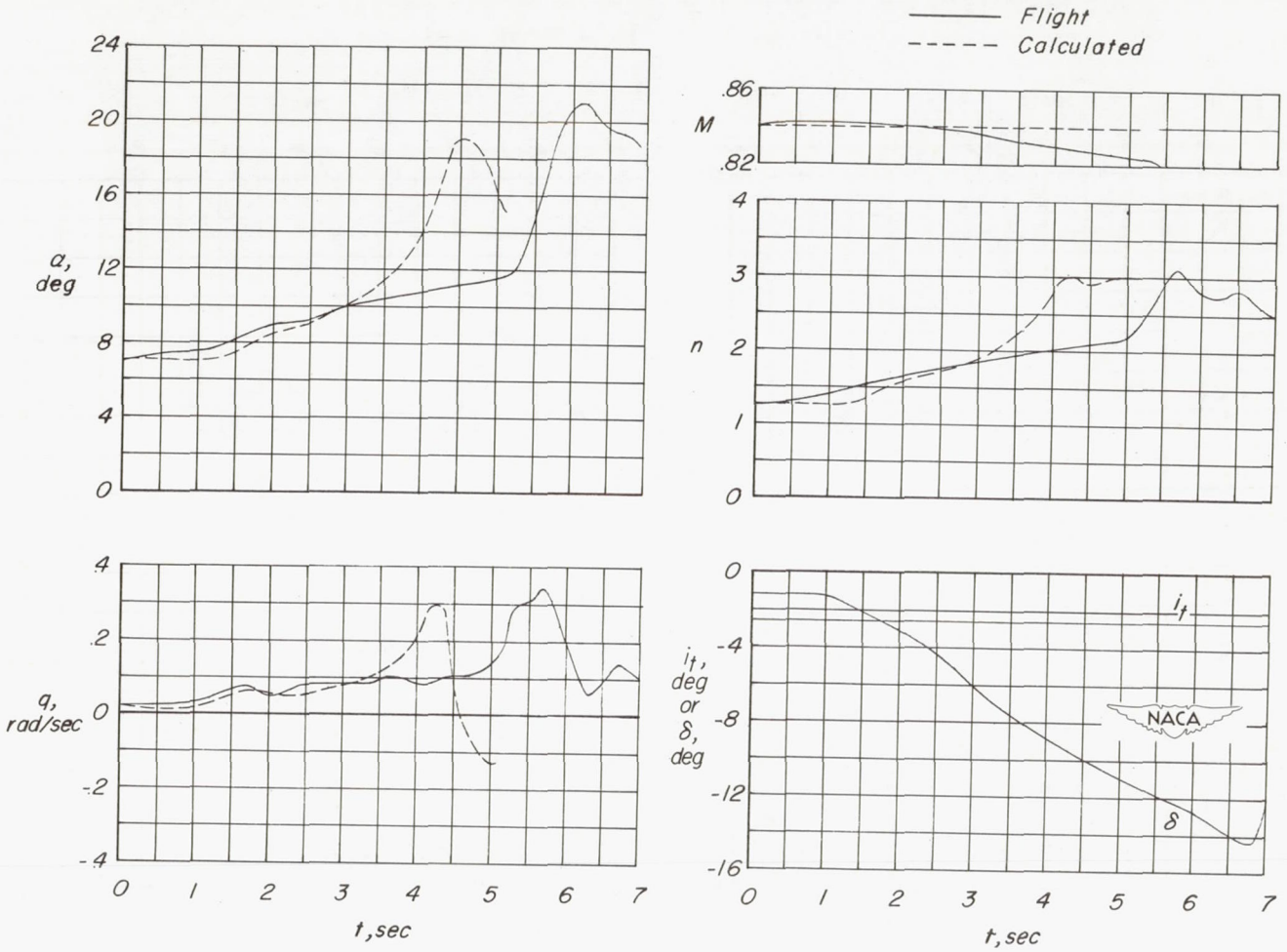
(c) $M_0 = 0.91$; $h_p = 41{,}000$ ft.

Figure 21.- Concluded.



(a) $M_0 = 0.76$; $h_p = 41{,}500$ ft.

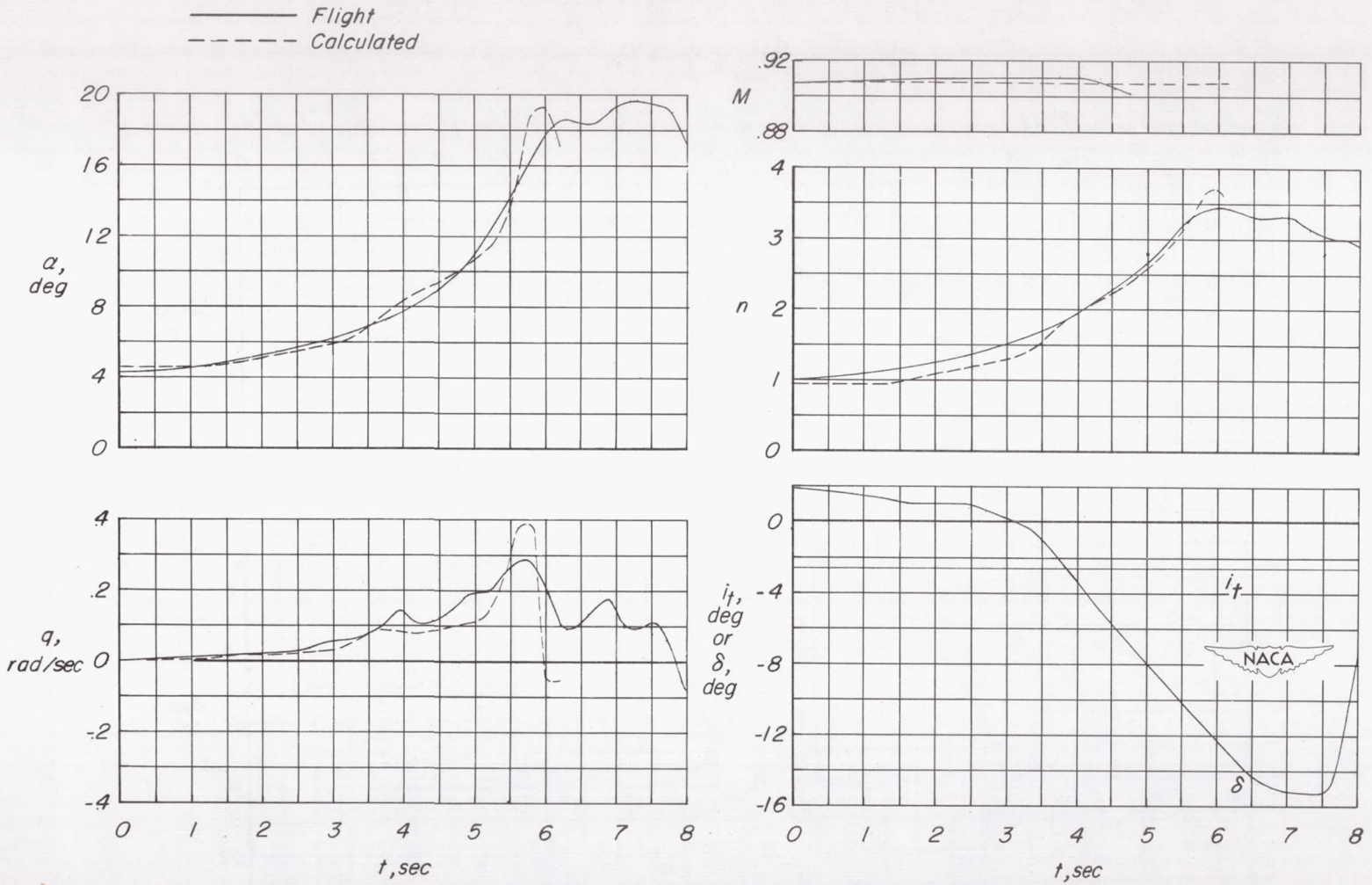
Figure 22.- Comparison of calculated and flight time histories for accelerated turns.



(b) $M_0 = 0.84$; $h_p = 39{,}500$ ft.

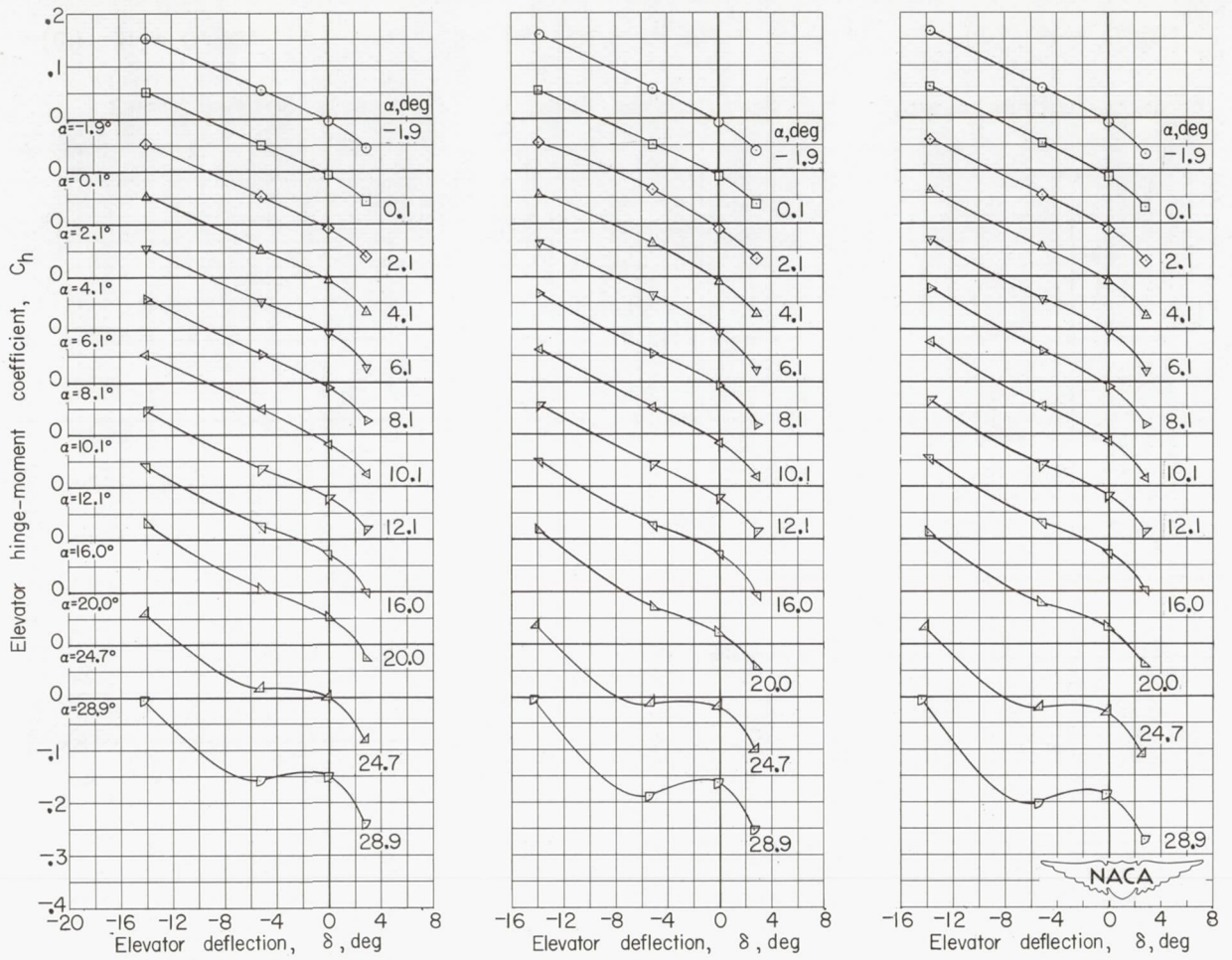
Figure 22.- Continued.

CONFIDENTIAL



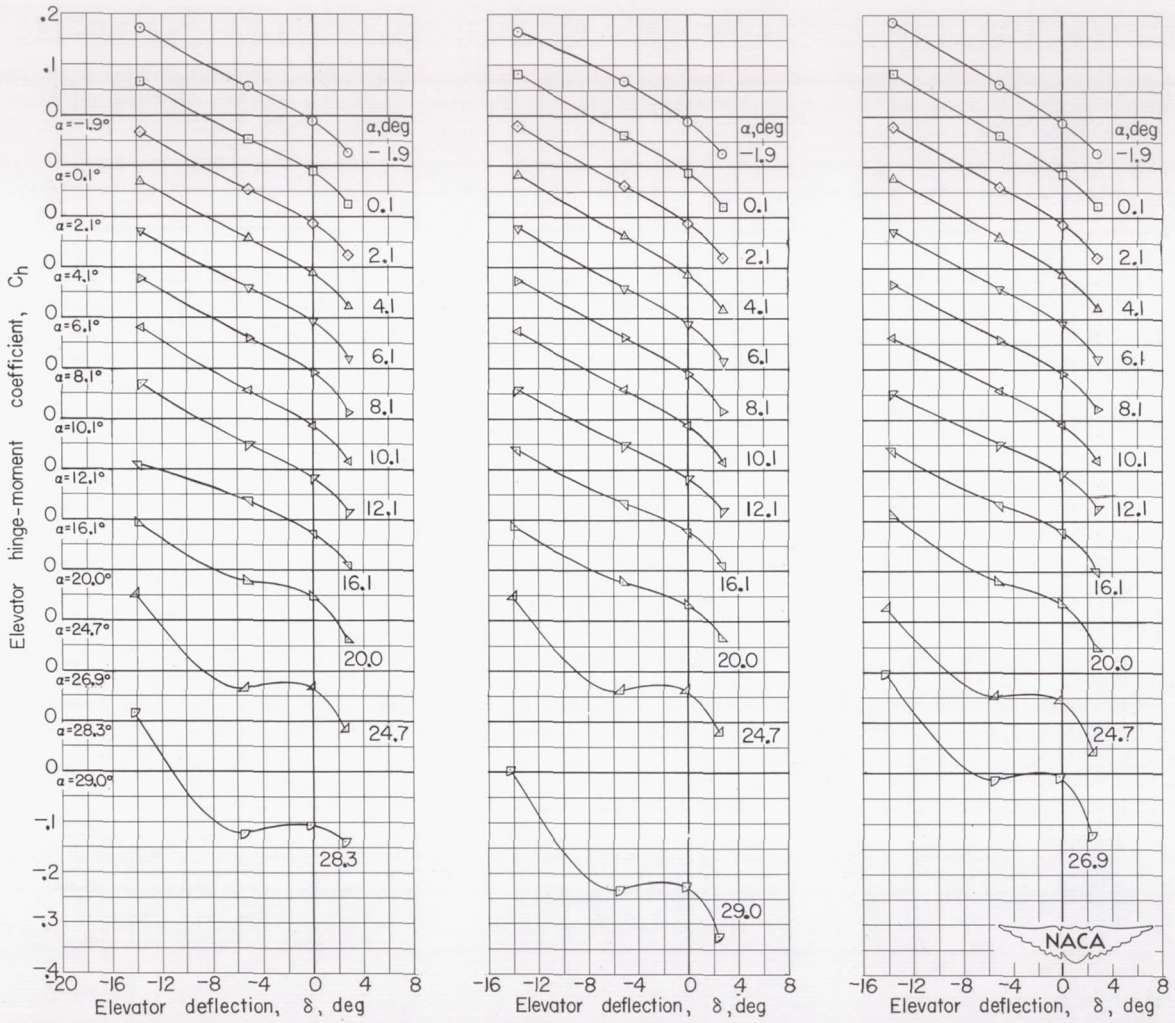
(c) $M_0 = 0.91$; $h_p = 38{,}500$ ft.

Figure 22.- Concluded.



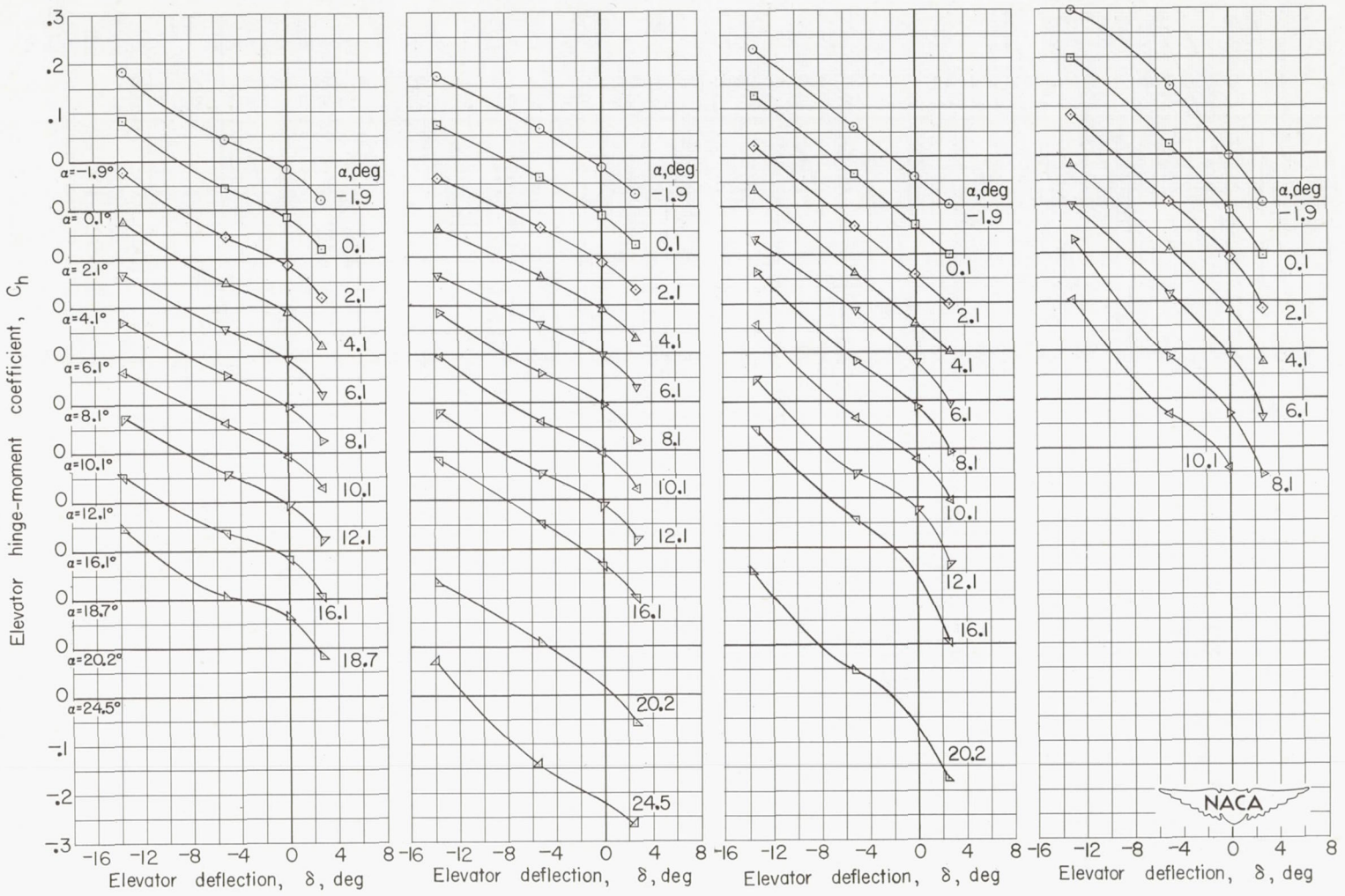
(a) M = 0.60. (b) M = 0.75. (c) M = 0.85.

Figure 23.- Variation of elevator hinge-moment coefficient with elevator deflection. $i_t = -1.7°$.



(d) M = 0.90. (e) M = 0.93. (f) M = 0.96.

Figure 23.- Continued.



(g) M = 1.00. (h) M = 1.03. (i) M = 1.06. (j) M = 1.10.

Figure 23.- Concluded.

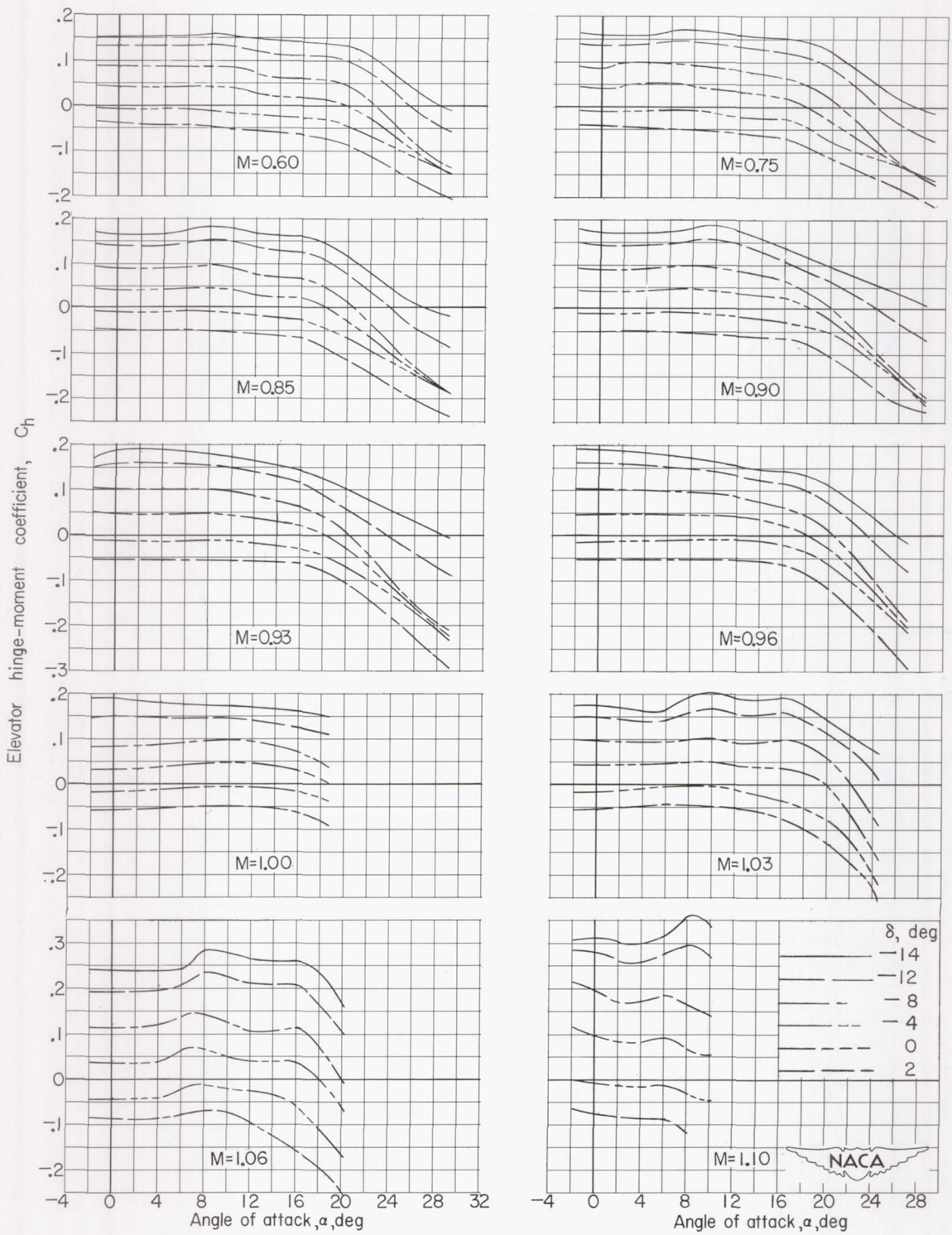


Figure 24.- Variation of elevator hinge-moment coefficient with angle of attack. $i_t = -1.7^\circ$.

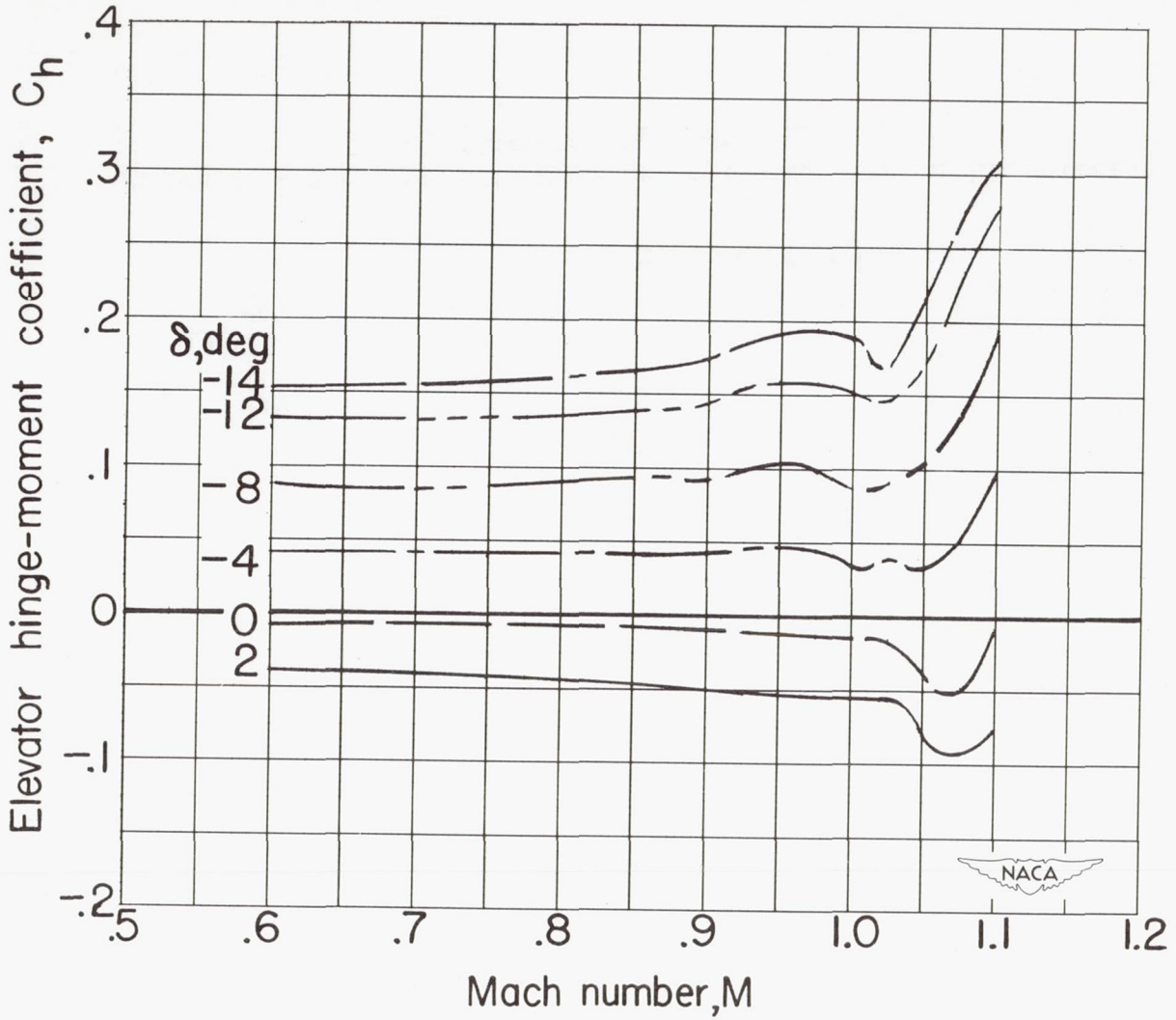


Figure 25.- Variation with Mach number of the elevator hinge-moment coefficient. $\alpha = 0^{\circ}$; $i_t = -1.7^{\circ}$.

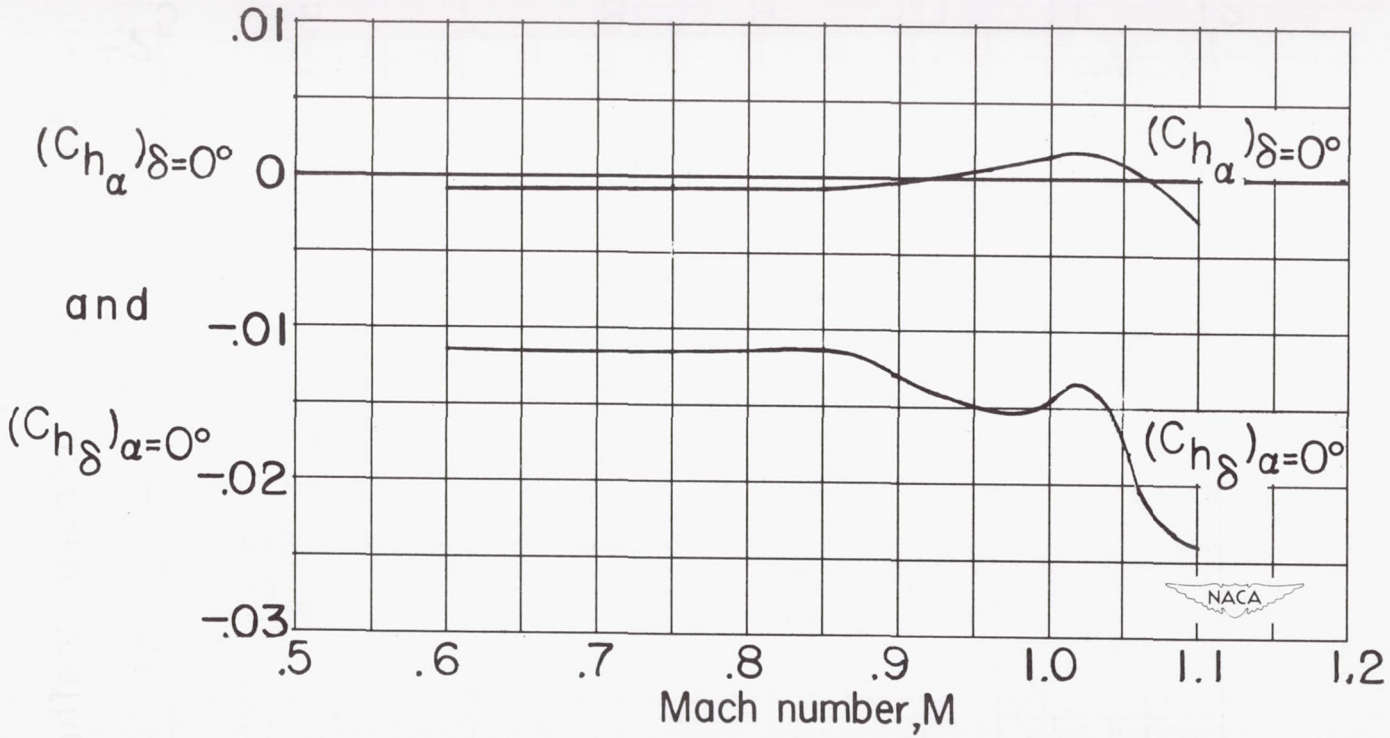


Figure 26.- Variation with Mach number of the elevator hinge-moment parameters C_{h_α} and C_{h_δ}.

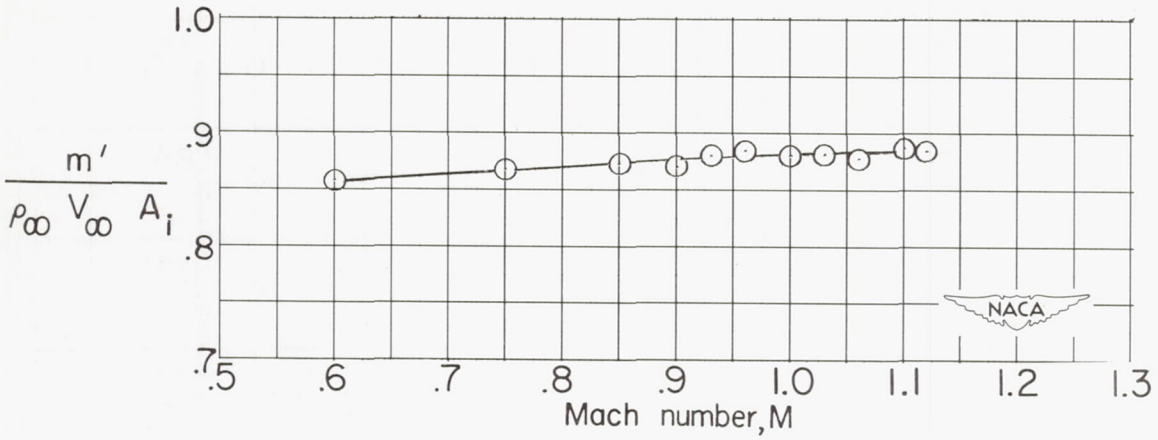


Figure 27.- Variation of the mass-flow ratio with Mach number. $\alpha = 0^\circ$.

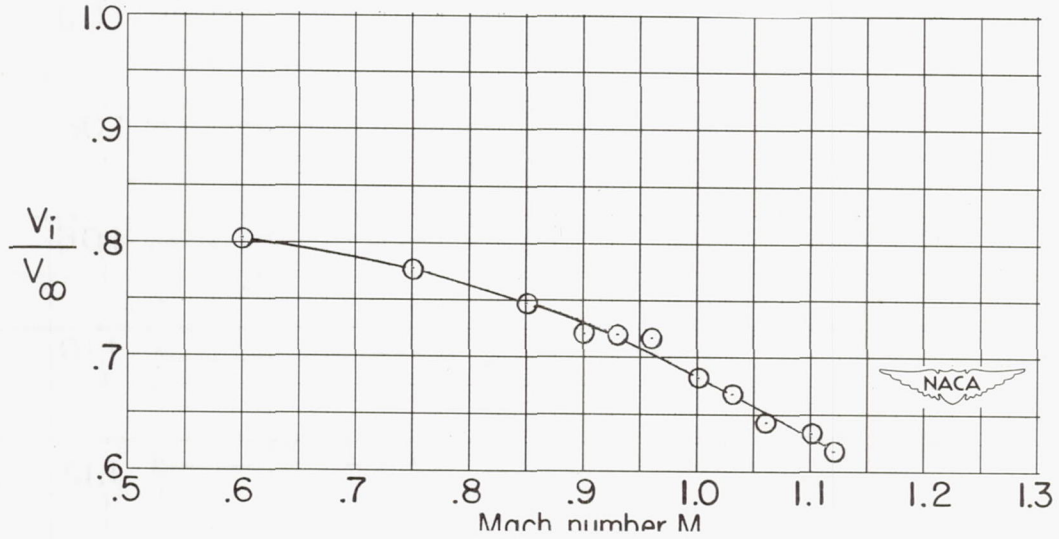


Figure 28.- Variation of inlet velocity ratio with Mach number. $\alpha = 0^\circ$.

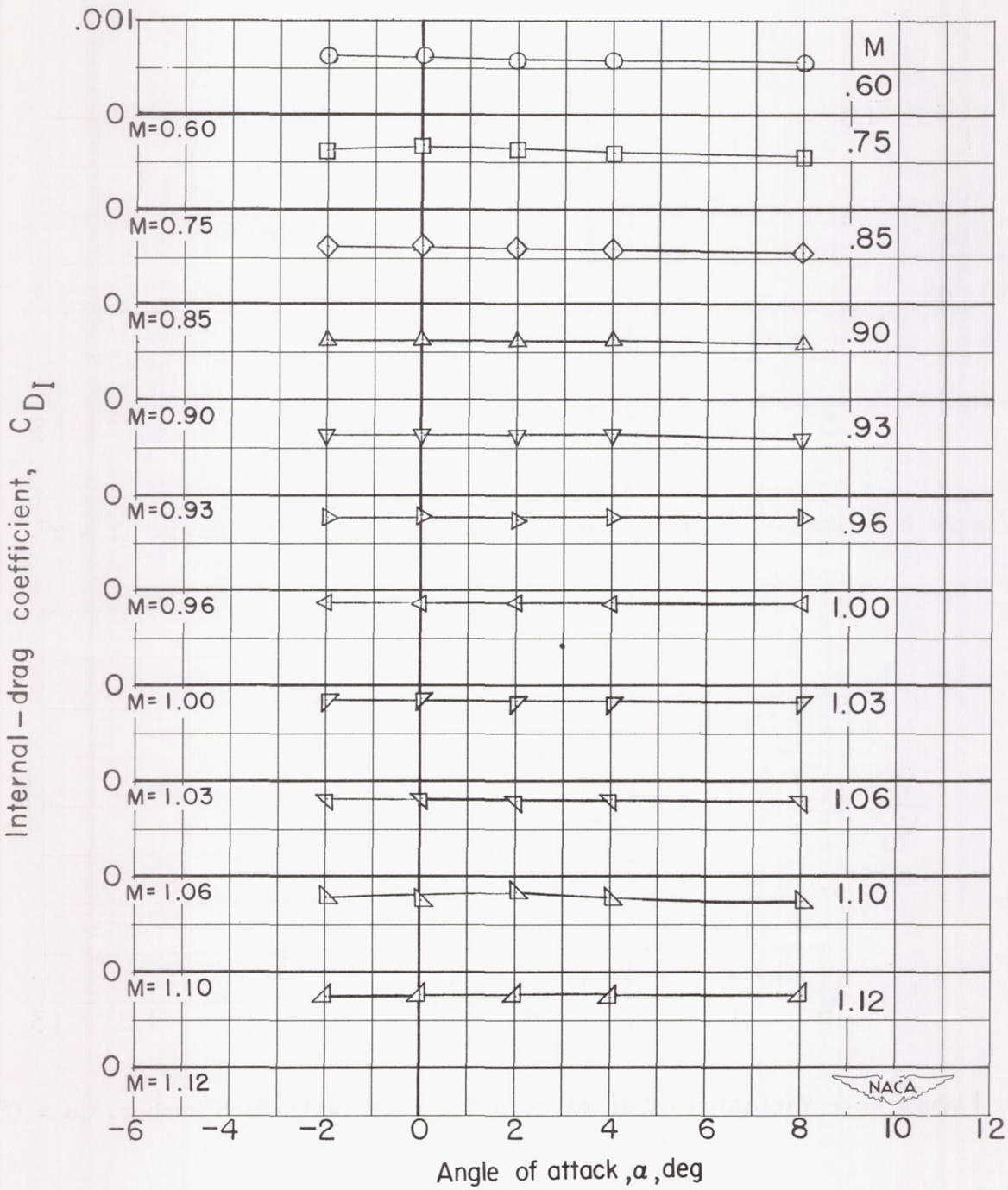
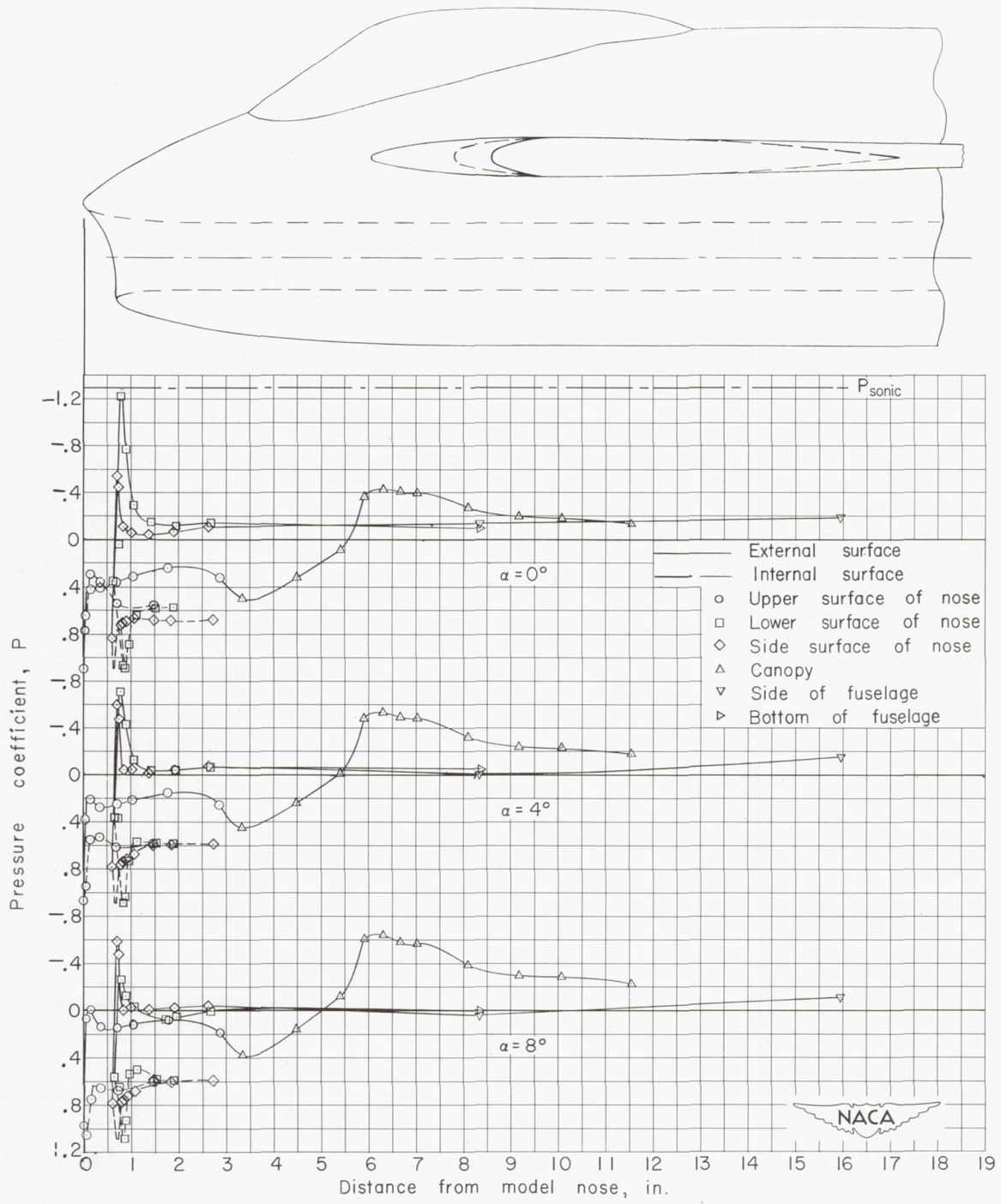
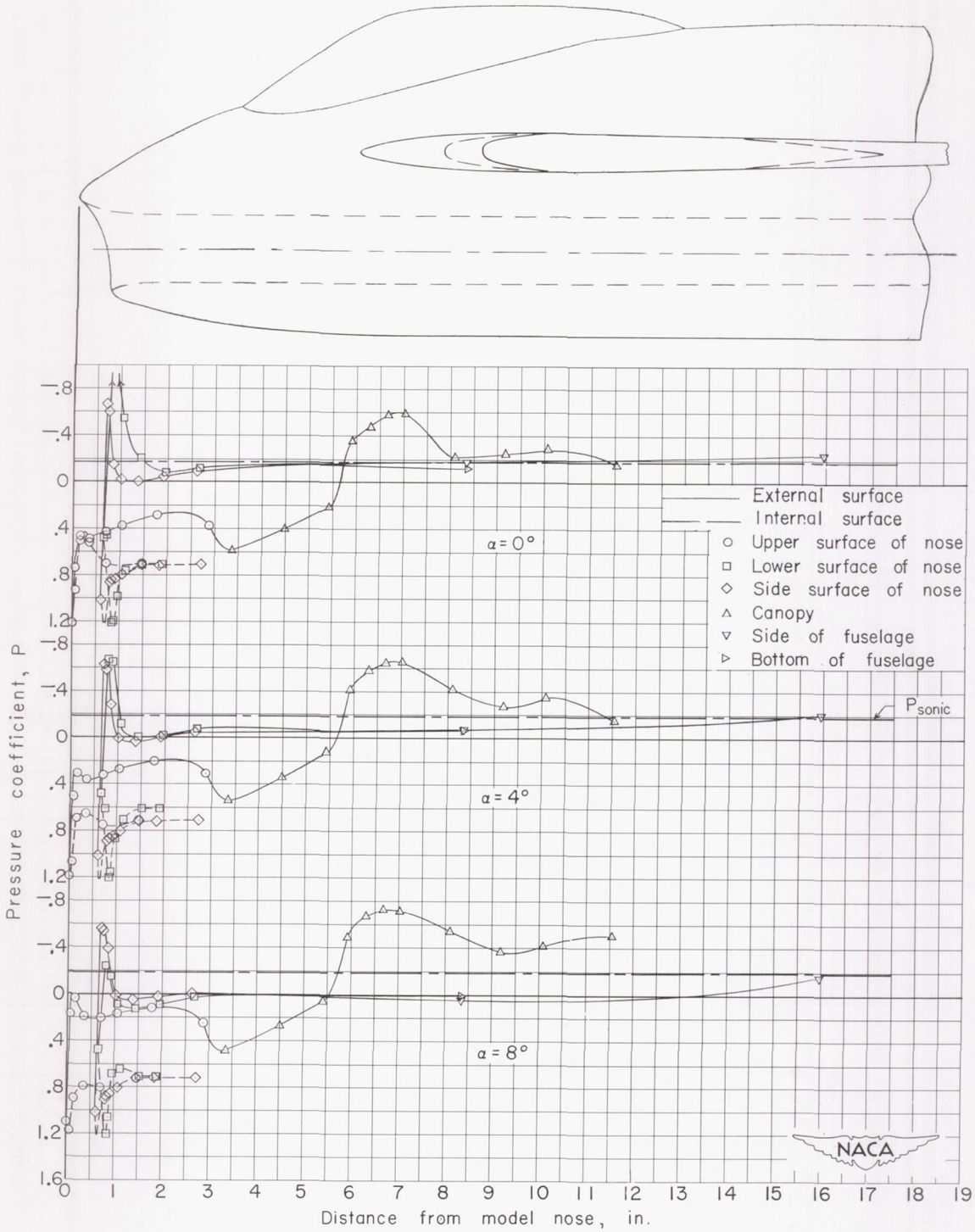


Figure 29.- Variation of internal-drag coefficient with angle of attack.



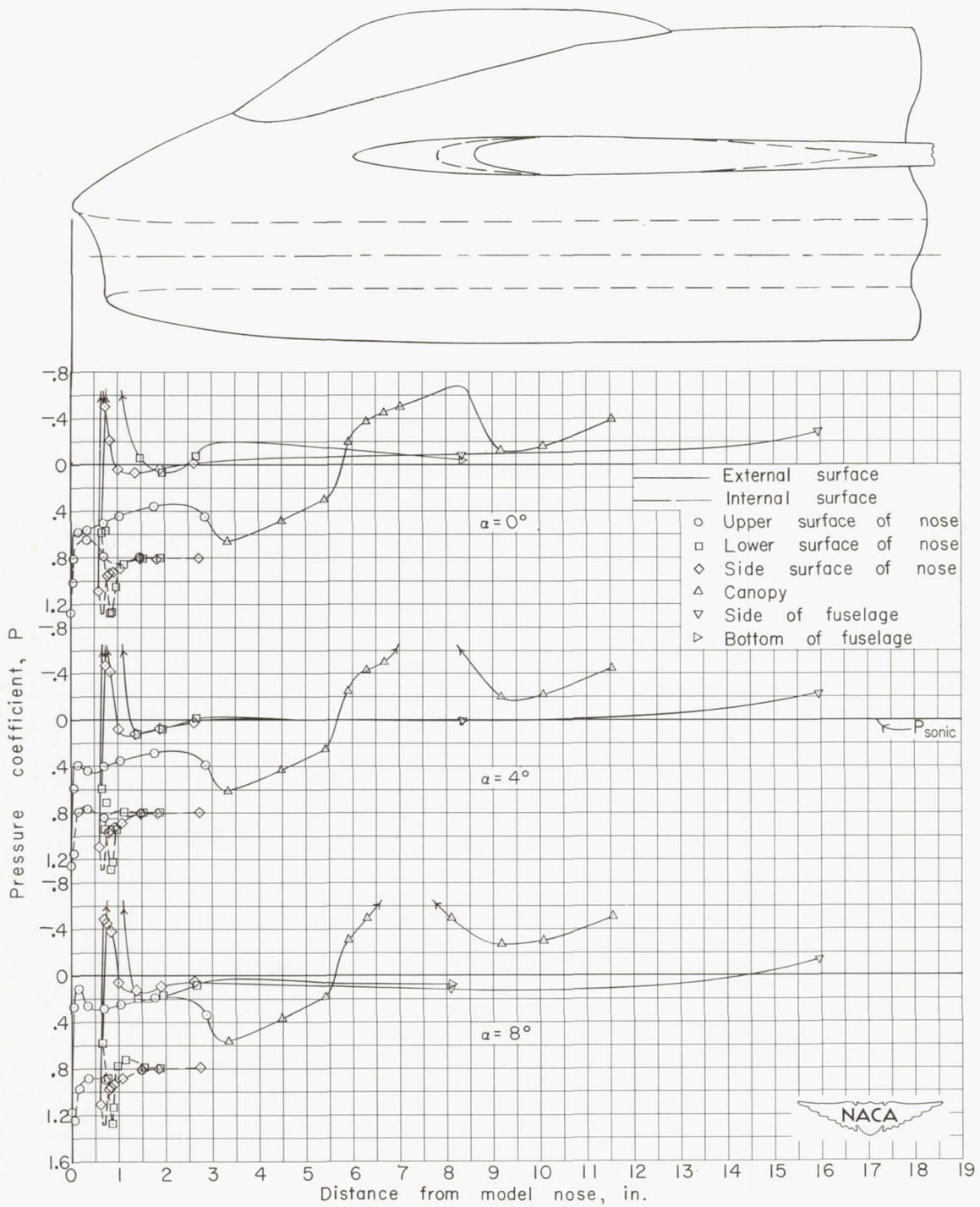
(a) M = 0.60.

Figure 30.- Surface pressure distributions over nose and canopy of model.



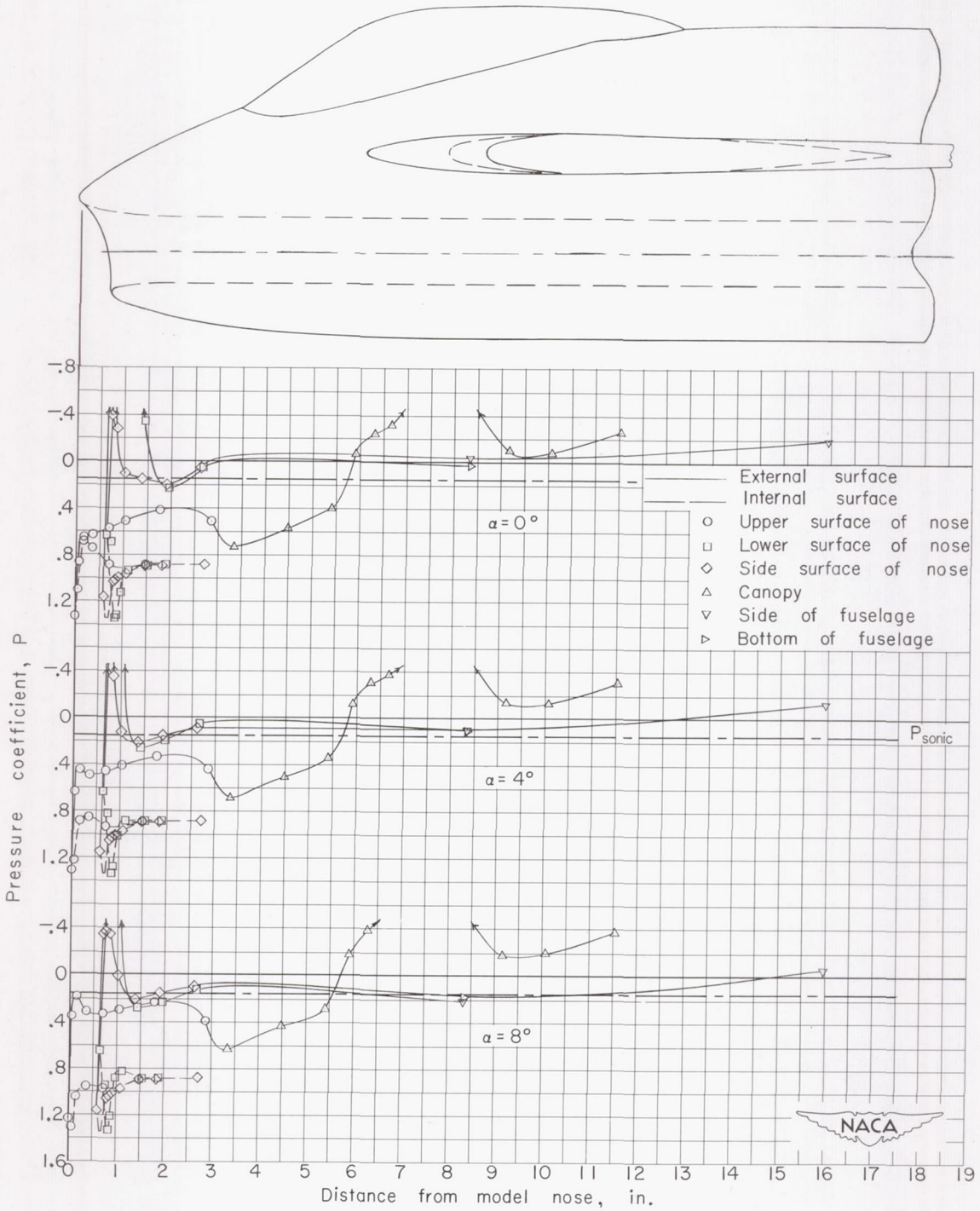
(b) M = 0.90.

Figure 30.- Continued.



(c) M = 1.00.

Figure 30.- Continued.



(d) M = 1.10.

Figure 30.- Concluded.

NACA-Langley - 10-28-53 - 325